Quaternary Science Reviews 165 (2017) 111–126

Contents lists available at ScienceDirect

Quaternary Science Reviews

journal homepage: www.elsevier.com/locate/quascirev

Last glacial tephra layers in the Talos Dome ice core (peripheral East Antarctic Plateau), with implications for chronostratigraphic correlations and regional volcanic history

Biancamaria Narcisi [a, *], Jean Robert Petit [b], Antonio Langone [c]

[a] ENEA, C.R. Casaccia, Roma, Italy
[b] Univ. Grenoble Alpes, CNRS, IRD, IGE, F-38000, Grenoble, France
[c] IGG-CNR, UOS of Pavia, Italy

ARTICLE INFO

Article history:
Received 30 September 2016
Received in revised form
26 April 2017
Accepted 27 April 2017

Keywords:
Tephra layers
Antarctic ice cores
Last glacial period
Millennial-scale climate variability
Volcanic glass composition
Northern Victoria Land volcanism
Explosive eruptions

ABSTRACT

Tephra isochrons offer considerable potential for correlating diverse palaeoarchives and highlighting regional climatic differences. They are especially useful when applied to polar ice records encompassing the last glacial, as these clearly portray the pronounced millennial-scale climate variability that characterised this period. Here we present the continuous record of primary fallout tephra layers in the East Antarctic Talos Dome ice core (72°49′S, 159°11′E), developed upon examination of the core sections spanning the glacial period 16.5 to 71 ka. A total of ca. 45 discrete tephra deposits precisely positioned stratigraphically relative to the temperature record for the core and dated using the AICC2012 timescale, were identified. Quantitative grain size, particle morphology, major and trace element composition using Coulter Counter, SEM, EPMA-WDS, and LA-ICP-MS analytical methods were studied as diagnostic features for tephra characterisation. The tephrostratigraphic framework provides a reference for future precise comparison between ice and sediment sequences across the Antarctic continent. Indeed, several potential markers characterised by distinct volcanic glass geochemistry and/or particular stratigraphic location (e.g., a 17.6-ka ash layer deposited during the well-known major acidity event) are now available for the direct linkage of palaeoclimatic archives. The Talos Dome tephra sequence, dominated by mid-distal pyroclastic products from the nearby Northern Victoria Land volcanoes, also represents the most comprehensive and best time-constrained record of regional Antarctic volcanism yet developed. It documents nearly continuous sustained explosive activity during the considered time interval and, combined with previous ice-core tephra results for the last and the current interglacial periods, suggests progressive compositional shift through time.

1. Introduction

A few decades after the pioneering work of S. Thorarinsson (1981), and particularly with the advent of analytical techniques for the characterisation of fine-grained single volcanic particles, tephra studies have become one of the most powerful tools in Quaternary research (Lowe, 2011, and references therein). Due to virtually instantaneous deposition of volcanic ash, and especially when the material exhibits distinctive features and regionally extensive distribution far beyond the volcanic edifice, this method has unique capabilities to establish accurate correlations between diverse and distant archives and to improve the chronology of past environmental changes. In addition to chronostratigraphic tasks, the tephra approach provides important constraints on frequency, style and composition of past volcanic activity that are essential for predicting future volcanic hazards, particularly in contexts as glaciated regions where pyroclastic deposits in the source area may not be available (Ponomareva et al., 2015, and references therein; Smellie, 1999).

Polar ice sequences hold valuable information on past climates and volcanism (Robock, 2000; Sigl et al., 2015). TALDICE (72°49′S, 159°11′E; 2315 m), the long ice core drilled at Talos Dome with the aim of documenting the regional variability of Antarctic palaeoclimate, preserves a significant tephra archive due to its mid-distal location relative to regional explosive volcanism, overall good quality of the core and unmodified stratigraphic order, and robust

* Corresponding author.
E-mail address: biancamaria.narcisi@enea.it (B. Narcisi).

http://dx.doi.org/10.1016/j.quascirev.2017.04.025
0277-3791/

independent dating of tephras and of various proxies for past changes (Fig. 1). The high accumulation rate of this East Antarctic core site (~80 mm water equivalent per year) relative to more inland locations of the Plateau provides an ideal location for developing a well-resolved record of primary fallout. Earlier studies have focused on the Holocene (Narcisi et al., 2001, 2012) and the Eemian interglacial section (Narcisi et al., 2016) and preliminary findings of the 70 ka volcanic record have also been reported (Narcisi et al., 2010a). These studies have shown the potential of this core for developing a tephrostratotype record for the Ross Sea sector of the Antarctic region. Northern Victoria Land volcanoes, located within a radius of ~250 km from Talos Dome (Fig. 1c) and associated with the active West Antarctic Rift System, are the major tephra contributors. These volcanoes were the site of volcanic activity of alkaline character over Quaternary times (Wörner, 1999).

This paper presents the inventory of tephra layers deposited in the last glacial between 17 and 64 ka BP. This is a period characterised by strong millennial-scale climate variability identified worldwide including polar ice sheets from both hemispheres (Blunier and Brook, 2001; Wolff et al., 2010). Specifically, the Antarctic temperature record appears punctuated by several warm events named Antarctic Isotope Maxima (AIM) that are obviously coupled with the Greenland Dansgaard-Oeschger events by the "bipolar see-saw" mechanism (EPICA Community Members, 2006; Landais et al., 2015; WAIS Divide Project Members, 2015). Important regional differences notwithstanding, this temperature pattern is clearly recorded also in the Talos Dome ice core as a direct response to the Greenlandic record (Stenni et al., 2011; Buiron et al., 2012) (Fig. 1). As such, the TALDICE tephra record of this critical period is of interest, given the prospects for identifying well-constrained tephra markers for confident stratigraphic correlations. The ultimate goal of tephra investigations is the independent alignment of diverse palaeoclimatic records in order to compare the expression of the rapid climatic events in different sectors of the Antarctic region. The tephra approach was already successfully employed to link last glacial proxy signals in Greenland ice cores and in Atlantic marine sediments (e.g. Davies et al., 2010). Moreover, since the available information for the activity of the local Antarctic volcanoes is very fragmentary for the investigated time period (e.g. Kyle, 1982), the present study aims to add to palaeovolcanic knowledge through an accurate temporal and compositional perspective.

2. Materials and analytical techniques

This investigation focuses on the ice core sections between 800 and 1300 m depth (Fig. 1) that were drilled during the 2006-07 field season. 43 deposits were considered and characterised (Supplementary Table 1). The majority of studied layers were located during core logging and processing as visually distinguishable from clear embedding ice. Their macroscopic appearance, showing a wide range of colour and thickness, was routinely documented with pictures (Supplementary Fig. 1). A few volcanic horizons too faint to show up to the naked eye (<1 mm thick) were identified during Coulter Counter (CC) granulometric measurements for continental dust studies. These samples showed anomalous features either as mass concentration or as grain size values, compared to typical aeolian dust in East Antarctic ice (e.g. Albani et al., 2012; Narcisi et al., 2010a) and through subsequent microscopic observations they proved to contain significant concentrations of well-preserved glass shards. No systematic search for crypto-tephra deposits was carried out in the present study, but this is planned for the near future.

The ice core sub-samples containing tephra layers were processed for ash recovery following laboratory protocols suited for the typically low concentration of volcanic particles in Antarctic tephras as well as their fine grain size, and successfully employed in former ice-core studies (e.g. Delmonte et al., 2002; Narcisi et al.,

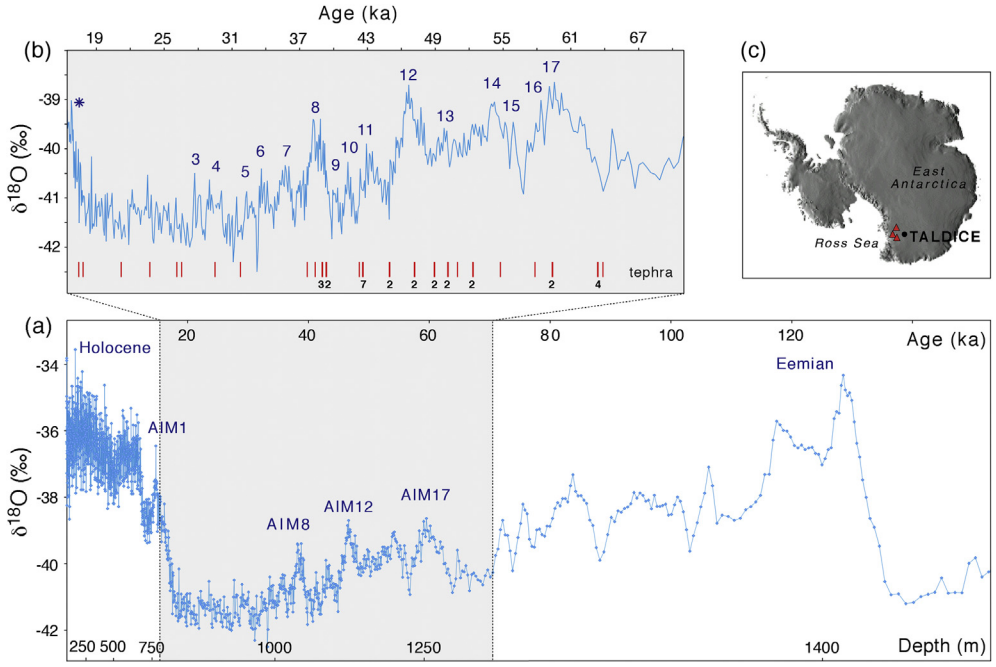

Fig. 1. (a) 1-m TALDICE stable isotope profile (Stenni et al., 2011) related to last glacial-interglacial climatic cycle vs. AICC2012 age (Veres et al., 2013) and depth, with the main climatic events indicated. Shading highlights the interval studied within this work. (b) Stratigraphic position of the tephra layers identified in this work (red bars, with indication of the number of closely timed horizons) relative to the $\delta^{18}O$ record vs. age. AIM climatic events (blue numbers) and the 'fluoride main event' (asterisk) are marked. (c) Satellite image of Antarctica with location of the ice core and local volcanoes. (For interpretation of the references to colour in this figure legend, the reader is referred to the web version of this article.)

2012, 2016). In brief, sample manipulation and processing were carried out in class 100 clean conditions. After decontamination of ice pieces by repeated washings and melting at room temperature, as a routine an aliquot of meltwater from each sample was devoted to quantitative measurements of grain size and concentrations using CC techniques (Delmonte et al., 2002). Volcanic ash recovery was attained by filtration through nucleopore polycarbonate membranes. A particle-bearing filter was embedded into epoxy resin and polished for subsequent grain-specific geochemical analysis.

The following suite of methods for single grain characterisation was used: (1) scanning electron microscopy (SEM) equipped with an energy dispersive X-ray spectrometer (EDS) for inspection of external shape and texture of unpolished particles and initial screening for geochemical analysis; (2) wavelength dispersive X-ray spectrometry (WDS) (working conditions as in Narcisi et al., 2012) for quantitative major element analysis of single polished particles; (3) laser ablation (LA)-ICP-MS (working conditions as in Narcisi et al., 2016) for complementary trace element analysis of individual glass shards from selected samples.

Our tephrostratigraphy is presented alongside the $\delta^{18}O$ record of the core (Fig. 1). This record is a proxy for temperature and provides robust chrono-stratigraphic constraints for each volcanic deposit. The TALDICE profile was reconstructed from measurements of water stable isotope composition with a depth resolution of 1 m, that for the considered period corresponds to a mean temporal resolution of ca. 90 years (Stenni et al., 2011; Buiron et al., 2012). Current dating of the TALDICE record derives from the Antarctic Ice Core Chronology 2012 (AICC2012), a timescale based on glaciological inputs and various data constraints that was developed coherently for four Antarctic ice cores including Talos Dome, alongside the Greenlandic NGRIP record (Veres et al., 2013). According to this timescale, the investigated core sections span the period between 16.5 and 71 ka (Fig. 1b).

For chemical classification purposes (Rickwood, 1989, and references therein) and for comparison between samples and with literature data, only major element analyses showing total oxide sums $\geq$ ~95 wt % were considered, and normalised to 100% total oxide values (Table 1) before use. Around 400 individual microprobe analyses are presented in the following sections (Fig. 2). The published data taken into account for interpretation and discussion include typical volcanic rock and mineral compositions of Antarctic sources. Presentation of potential source volcanoes for the study area and related critical overview of existing data can be found in Del Carlo et al. (2015); Narcisi et al. (2010a, 2016). Moreover, we considered Antarctic tephra records spanning the same time interval of TALDICE for potential one-to-one tephra correlations. A handful of ice sequences from the Antarctic Plateau sectors facing the Ross Sea and the East Pacific Ocean are suitable for comparison (Curzio et al., 2008; Dunbar et al., 2008; Dunbar and Kurbatov, 2011). Note that the deep ice cores retrieved from the inner East Antarctic Plateau are dominated by volcanic ash sourced in the South Atlantic region (Narcisi et al., 2010b). Marine sediment records from the Ross Sea (Del Carlo et al., 2015; Licht et al., 1999) and the Scotia Sea (Xiao et al., 2016) are unsuitable for our correlation purpose because the identified tephra layers are not adequately constrained for either chronostratigraphy or glass geochemical composition.

3. Results and discussion

3.1. Origin of the tephras

Several lines of evidence indicate that the examined tephras originate from Mt. Melbourne, The Pleiades and Mt. Rittmann volcanoes, located in Northern Victoria Land some 200 km from the Talos Dome core site. First, the morphology of the glass pyroclasts examined by microscopic inspection shows various shapes and degrees of vesiculation, but generally is suggestive of atmospheric fallout from volcanic plumes related to explosive eruptions (Supplementary Fig. 2). Second, Talos Dome lies in a favourable position for aeolian transport with respect to Northern Victoria Land volcanoes (Sala et al., 2008; Scarchilli et al., 2011) and therefore is prone to receive airborne tephra. Indeed, the majority of the studied layers are prominent to the naked eye (Supplementary Fig. 1), and the preserved volcanic material is reasonably coarse-grained, indicating fairly proximal deposition. Particle concentration and total tephra fallout are also high (Supplementary Table 1; Figs. 3–9) and inconsistent with typical atmospheric dust load onto Talos Dome and other sites of the Central East Antarctic Plateau (e.g. Albani et al., 2012). As for major element geochemistry, the juvenile glass microprobe results plotted on the total alkali-silica (TAS) classification diagram indicate that the tephras range in composition from basalt to rhyolite (Table 1 and Fig. 2a). Several samples are classified as trachytes. Tephra compositions define a coherent alkaline trend typical of extensional tectonic settings and broadly congruent with published rock compositions of the Northern Victoria Land volcanoes (Fig. 2a). Glass shard compositions are also consistent with those of TALDICE tephra layers occurring in other core sections, that were positively compared with specific volcanic products sourced in the Victoria Land province (Narcisi et al., 2012, 2016). This suggests that the local volcanoes represent the major tephra contributors in the studied time interval as well as in other periods previously explored. Furthermore, although our geochemical study focuses on glass geochemistry as being the most compelling criterion for tephra fingerprinting, ancillary evidence for tephra attribution comes from compositional data of free feldspar crystals that were occasionally encountered during microprobe analysis (Fig. 2b). The mineral composition is predominantly anorthoclase or sanidine and is consistent with those in Northern Victoria Land volcanics.

Besides identification of source for volcanic materials, glass shards generally display well-preserved textures (Supplementary Fig. 2), indicating that soon after eruption they were rapidly incorporated into the snow series with no significant depositional reworking. Each individual layer thus provides a time stratigraphic horizon reliably documenting a dated explosive event and allowing stratigraphic correlation.

3.2. The TALDICE tephra record

In the following sections, we provide the description (chronostratigraphic position, physical properties, geochemistry) of the individual layers forming the TALDICE tephra catalogue for the studied glacial period (Supplementary Table 1). Detected layers are presented in order of increasing depth/age. For clarity, and in order to highlight the significance of their stratigraphic position, the layers are grouped according to the climatic events within (or close to) which they were deposited. Climatic events not recording tephra layers are omitted. Geochemical data are reported in Table 1 and in Supplementary Tables 2–3. Sample details are illustrated in Figs. 3–10.

3.2.1. Last deglaciation and the Last Glacial Maximum

In this work, two prominent layers, labelled TD822 and TD828, respectively, were identified in the sections recording the climate transition from the last glacial to the present interglacial (Fig. 3a). Two further layers (TD783 and TD779, dated 15.54 ± 0.38 ka and 15.36 ± 0.38 ka, respectively, according to AICC21012) previously presented by Narcisi et al. (2012) occur higher in the core within the

Table 1
Major element composition of glass shards from TALDICE tephra horizons determined by electron microprobe analysis. Data in weight percent (wt%) are recalculated to a sum of 100 wt% and are presented as mean and one standard deviation of *n* analyses of different glass shards. Original oxide totals before recalculation are also given. Total iron expressed as FeO. -a, -b, etc. denote separate populations of glass inside samples. Based on measurements of reference glasses, typical analytical errors (RSD) are as follows: <1% for SiO_2; 1–2% for CaO, Al_2O_3, K_2O; 2–3% for FeO; 3–6% for MnO, TiO_2; 2–9% for NaO_2 and MgO. Rock type after TAS plot (Rickwood, 1989, and references therein). Age of tephras are based on AICC2012 timescale (Veres et al., 2013).

TD sample	Age (ka)	*n*	SiO_2	TiO_2	Al_2O_3	FeO_{tot}	MnO	MgO	CaO	Na_2O	K_2O	Original total	Rock type
822-a	17.61 ± 0.73	13	59.72	0.80	18.40	6.01	0.19	0.93	2.69	6.36	4.90	98.10	trachyte
		SD	0.32	0.07	0.36	0.45	0.02	0.09	0.16	0.48	0.20	1.01	
822-b	17.61 ± 0.73	1	61.08	0.60	18.56	5.23	0.17	0.59	2.03	6.32	5.41	97.40	trachyte
822-c	17.61 ± 0.73	1	62.85	0.37	18.09	4.55	0.16	0.27	1.51	6.46	5.75	95.75	trachyte
822-d	17.61 ± 0.73	1	62.98	0.38	18.57	4.77	0.20	0.28	1.38	5.79	5.64	97.35	trachyte
828-a	18.00 ± 0.82	4	58.69	0.96	17.48	7.68	0.26	1.06	2.61	6.68	4.60	99.05	trachyte
		SD	0.91	0.05	0.43	0.34	0.02	0.05	0.43	0.60	0.68	1.25	
828-b	18.00 ± 0.82	3	61.93	0.56	18.92	4.09	0.12	0.52	2.88	6.41	4.57	99.23	trachyte
		SD	0.80	0.19	1.07	1.42	0.03	0.25	0.20	0.45	0.48	0.69	
828-c	18.00 ± 0.82	1	61.32	0.59	18.42	5.60	0.25	0.58	1.06	7.30	4.87	99.66	trachyte
828-d	18.00 ± 0.82	1	63.59	0.54	18.28	3.98	0.11	0.44	1.10	6.16	5.80	97.53	trachyte
891	21.55 ± 1.15	12	48.26	3.78	15.64	10.55	0.21	5.34	10.55	4.18	1.48	98.11	trachybasalt
		SD	1.16	0.55	0.67	1.09	0.21	0.56	1.09	0.97	0.25	1.31	
914	21.16 ± 0.71	15	68.40	0.30	15.74	4.08	0.13	0.09	1.42	4.72	5.12	99.27	trachyte
		SD	0.27	0.02	0.23	0.09	0.02	0.02	0.05	0.28	0.20	0.72	
949	29.73 ± 0.66	6	61.89	0.31	16.19	7.00	0.28	0.05	0.95	8.57	4.76	98.65	trachyte
		SD	0.31	0.03	0.52	0.37	0.02	0.02	0.03	0.39	0.31	1.06	
970	31.72 ± 0.66	23	67.55	0.30	16.17	4.19	0.13	0.08	1.45	4.87	5.26	98.86	trachyte
		SD	0.44	0.02	0.29	0.12	0.02	0.02	0.05	0.33	0.18	1.22	
1050	38.45 ± 0.48	5	68.46	0.41	14.94	4.96	0.16	0.04	1.22	4.82	4.99	98.86	trachyte
		SD	0.37	0.04	0.14	0.30	0.02	0.02	0.12	0.26	0.37	0.66	
1058	38.96 ± 0.48	4	66.47	0.47	15.64	4.66	0.17	0.21	1.37	5.47	5.54	98.47	trachyte
		SD	2.64	0.32	0.75	0.61	0.02	0.24	0.86	1.28	0.44	1.02	
1059Top-a	39.03 ± 0.48	4	63.13	0.40	17.79	4.60	0.19	0.34	1.52	6.62	5.41	99.46	trachyte
		SD	0.09	0.05	0.33	0.40	0.02	0.08	0.36	0.35	0.60	0.16	
1059Top-b	39.03 ± 0.48	1	60.70	0.67	17.16	7.04	0.26	0.68	1.66	6.44	5.40	99.78	trachyte
1059Top-c	39.03 ± 0.48	1	62.89	0.55	16.38	6.29	0.25	0.47	1.69	6.32	5.16	98.45	trachyte
1059Bottom	39.03 ± 0.48	6	63.76	0.42	17.60	4.77	0.17	0.35	1.46	5.96	5.52	97.94	trachyte
		SD	0.59	0.05	0.19	0.28	0.03	0.07	0.07	0.32	0.21	1.62	
1067Bottom	39.56 ± 0.50	11	64.00	0.53	17.29	3.98	0.16	0.49	1.73	6.09	5.73	98.33	trachyte
		SD	0.61	0.17	0.54	0.46	0.04	0.15	0.31	0.49	0.64	1.48	
1099	42.00 ± 0.51	4	64.72	0.54	17.53	4.51	0.16	0.47	1.94	5.43	4.70	97.01	trachyte
		SD	1.55	0.30	1.03	1.34	0.07	0.28	0.63	1.17	0.43	1.81	
1105C	42.54 ± 0.52	7	47.45	3.19	16.10	10.59	0.17	5.97	11.49	3.45	1.61	97.64	trachybasalt
		SD	0.55	0.34	0.61	0.21	0.03	0.76	0.45	0.37	0.10	1.26	
1105D	42.54 ± 0.52	19	47.43	3.48	16.06	11.22	0.19	5.36	10.36	4.14	1.77	97.16	trachybasalt
		SD	0.80	0.55	0.46	0.66	0.02	0.91	1.14	0.49	0.26	1.27	
1105G	42.54 ± 0.52	26	48.08	3.23	15.77	10.82	0.18	5.66	11.05	3.63	1.57	98.49	trachybasalt
		SD	0.90	0.50	0.65	0.79	0.02	0.95	1.10	0.59	0.21	1.23	
1163	47.20 ± 0.52	*7*	61.52	0.45	17.41	5.50	0.25	0.31	1.15	7.96	5.44	98.65	trachyte
		SD	0.55	0.07	0.50	0.64	0.07	0.05	0.16	0.83	0.27	0.57	
1164	47.28 ± 0.60	*8*	66.79	0.27	15.81	5.07	0.18	0.02	1.20	5.71	4.96	98.66	trachyte
		SD	0.68	0.06	0.40	0.60	0.03	0.02	0.09	0.33	0.16	1.42	
1180	48.93 ± 0.70	*4*	61.57	0.36	17.38	5.94	0.24	0.17	0.87	8.08	5.39	97.75	trachyte-phonolite
		SD	0.67	0.03	0.55	0.64	0.03	0.02	0.11	0.76	0.22	2.67	
1183	49.30 ± 0.72	*12*	66.06	0.30	15.37	5.75	0.19	0.01	1.04	6.38	4.90	98.19	trachyte
		SD	0.53	0.03	0.51	0.29	0.02	0.01	0.16	0.49	0.24	1.58	
1189	50.02 ± 0.81	*8*	46.30	4.28	14.85	13.55	0.22	5.36	11.33	3.11	0.99	96.77	basalt
		SD	0.27	0.22	0.42	0.43	0.04	0.31	0.27	0.36	0.14	0.98	
1191	50.27 ± 0.86	*10*	55.10	2.28	16.67	8.14	0.22	2.17	4.98	6.00	4.44	97.90	tephriphonolite
		SD	1.74	0.32	0.44	0.77	0.03	0.44	0.93	0.76	0.59	1.26	
1197	51.04 ± 0.90	13	61.12	0.30	17.68	6.26	0.25	0.16	0.99	8.13	5.11	97.27	trachyte
		SD	0.64	0.06	0.37	0.36	0.03	0.06	0.15	0.73	0.33	1.47	
1208Top	52.43 ± 0.83	*17*	63.19	0.21	17.82	4.32	0.19	0.11	0.87	7.87	5.42	98.70	trachyte
		SD	1.70	0.09	0.32	1.48	0.07	0.05	0.20	0.50	0.44	1.19	
1208Bottom	52.43 ± 0.83	*10*	62.48	0.20	17.55	4.88	0.25	0.13	0.93	8.23	5.36	98.04	trachyte
		SD	1.68	0.05	0.90	1.44	0.14	0.06	0.15	1.05	0.38	0.94	
1226-a	54.76 ± 0.76	*5*	67.35	0.18	15.21	4.26	0.15	0.02	0.95	6.59	5.30	98.11	trachyte
		SD	1.35	0.04	0.71	1.33	0.05	0.01	0.28	0.98	0.34	1.36	
1226-b	54.76 ± 0.76	*1*	64.62	0.42	13.03	9.15	0.33	0.00	1.74	5.82	4.88	97.69	trachyte
1226-c	54.76 ± 0.76	*1*	64.98	0.27	12.71	8.66	0.34	0.06	1.81	6.20	4.97	95.82	trachyte
1226-d	54.76 ± 0.76	*1*	66.95	0.56	9.15	10.93	0.56	0.03	2.14	5.14	4.54	98.82	trachyte
1246-a	57.77 ± 0.95	*9*	69.63	0.23	14.27	4.52	0.01	0.01	0.74	5.59	4.87	97.42	rhyolite
		SD	0.86	0.03	0.96	0.63	0.01	0.01	0.15	0.47	0.11	0.47	
1246-b	57.77 ± 0.95	*1*	63.76	0.47	15.93	5.57	0.20	0.16	2.22	6.91	4.78	98.43	trachyte
1246-c	57.77 ± 0.95	*1*	67.19	0.40	14.18	5.46	0.17	0.03	1.04	6.41	5.13	97.30	trachyte
1257-a	59.40 ± 1.15	*4*	62.13	0.37	17.31	6.37	0.24	0.13	0.83	8.17	4.45	97.24	trachyte
		SD	0.49	0.19	0.38	0.78	0.04	0.08	0.16	0.51	0.53	1.53	
1257-b	59.40 ± 1.15	*1*	58.86	1.56	15.92	7.90	0.22	0.44	1.96	8.62	4.52	97.08	phonolite
1257-c	59.40 ± 1.15	*1*	62.48	0.68	16.86	6.37	0.20	0.57	2.11	5.58	5.15	100.27	trachyte

Table 1 (*continued*)

TD sample	Age (ka)	*n*	SiO_2	TiO_2	Al_2O_3	FeO_{tot}	MnO	MgO	CaO	Na_2O	K_2O	Original total	Rock type
1257-d	59.40 ± 1.15	*1*	64.32	0.29	18.41	3.04	0.12	0.19	1.67	7.44	4.53	98.60	trachyte
1258-a	59.55 ± 1.17	*10*	67.53	0.27	15.30	4.64	0.14	0.01	0.94	6.38	4.81	98.43	trachyte
		SD	0.59	0.06	0.77	0.94	0.05	0.01	0.13	0.43	0.14	0.97	
1258-b	59.55 ± 1.17	*1*	65.87	0.25	15.80	4.87	0.15	0.00	1.97	6.42	4.67	98.15	trachyte
1258-c	59.55 ± 1.17	*1*	66.19	0.21	15.19	5.05	0.15	0.02	2.21	6.65	4.34	98.80	trachyte
1278	63.35 ± 1.45	*4*	61.88	0.45	17.66	5.67	0.24	0.20	0.90	7.60	5.41	98.58	trachyte
		SD	1.41	0.07	0.53	1.26	0.07	0.05	0.16	0.98	0.42	1.42	
1279A-a	63.61 ± 1.44	*1*	45.97	3.64	16.57	11.15	0.24	4.35	10.80	4.64	2.64	95.93	tephrite
1279A-b	63.61 ± 1.44	*1*	52.46	3.28	15.61	10.37	0.18	3.29	7.03	4.70	3.09	98.02	basaltic trachyandesite
1279A-c	63.61 ± 1.44	*1*	58.62	0.71	17.11	8.94	0.33	0.95	2.96	6.34	4.04	97.29	trachyandesite
1279A-d	63.61 ± 1.44	*1*	59.01	0.71	16.50	9.03	0.32	0.84	2.96	6.17	4.46	96.11	trachyandesite
1279B-a	63.61 ± 1.44	*9*	63.64	0.50	17.71	4.38	0.15	0.48	2.06	5.94	5.13	97.25	trachyte
		SD	1.18	0.16	0.60	1.42	0.06	0.13	0.44	0.64	0.40	1.07	
1279B-b	63.61 ± 1.44	*1*	53.12	3.08	16.25	9.24	0.19	2.77	6.27	5.35	3.74	97.90	basaltic trachyandesite
1279C-a	63.61 ± 1.44	*10*	64.01	0.44	18.33	3.58	0.12	0.39	1.99	6.09	5.05	97.81	trachyte
		SD	1.03	0.17	0.96	1.41	0.05	0.16	0.72	0.68	0.59	1.52	
1279C-b	63.61 ± 1.44	*3*	46.18	3.67	16.69	11.27	0.23	4.66	10.60	4.34	2.36	96.73	tephrite
		SD	1.32	0.36	0.93	0.37	0.05	0.63	1.17	0.50	0.71	1.78	
1279C-c	63.61 ± 1.44	*1*	56.90	4.79	19.76	4.20	0.07	1.80	3.89	5.63	2.97	97.03	basaltic trachyandesite
1279C-d	63.61 ± 1.44	*1*	58.32	0.69	17.20	8.78	0.33	0.95	2.82	6.60	4.32	98.66	basaltic trachyandesite
1279C-e	63.61 ± 1.44	*1*	71.72	0.16	13.49	4.21	0.17	0.05	0.36	5.61	4.22	96.27	rhyolite

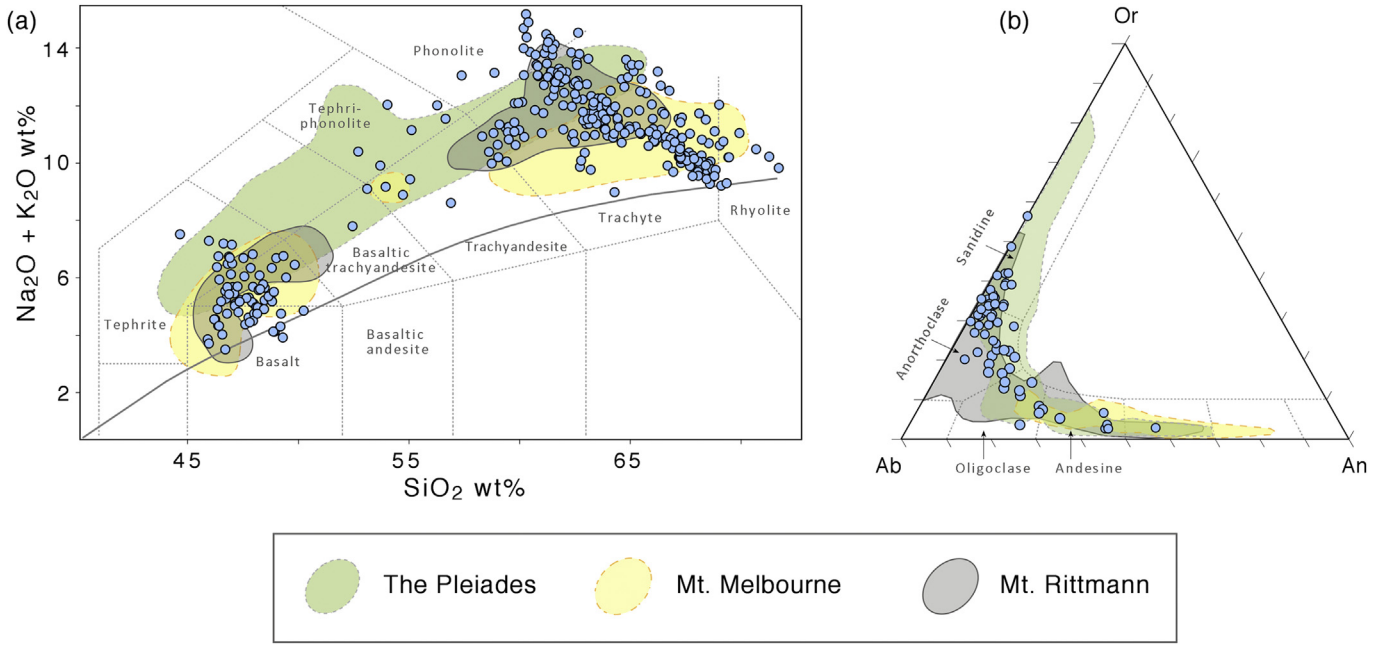

Fig. 2. Results of microprobe analysis of individual volcanic grains. Envelopes for the different volcanic sources are based on published data obtained mainly from bulk samples (The Pleiades: Kyle, 1982, 1986; Mt. Melbourne: Armienti et al., 1991; Giordano et al., 2012; Mt. Rittmann: Armienti and Tripodo, 1991). (a) Total alkali-silica (TAS) classification diagram (Rickwood, 1989, and references therein) showing glass-shard composition (330 individual analyses). (b) Ternary classification diagram for feldspars showing crystal composition (65 individual analyses).

deglaciation slope (Fig. 3a).

TD822 (17.61 ± 0.73 ka) forms a mm-thick greyish horizon composed mainly of poorly vesiculated glass shards up to about 40 μm in size. Thirteen microprobe analyses provide the composition of the main glass fraction (TD822-a), which is classified as trachyte (Fig. 3c). Further three individual shards (TD822-b to -d) are also trachytic but display different Mg, Ca and Fe oxide contents with respect to the main population and appear slightly more silicic (Fig. 3a and Table 1). Analysis of fifteen glass shards exhibits a peculiar trace-element signature more similar to studied basic samples than to trachytes (Fig. 10). Interestingly, TD822 is located within the 'fluoride main event', occurring in TALDICE core at ca. 820–825 m depth interval (Mirko Severi, personal communication, 2016) (Fig. 3a). This is a significant 2–3 centuries-long acidity event identified in ice cores from the East and West Antarctic ice sheets (Schwander et al., 2001 and references therein; Sigl et al., 2016) and representing an excellent chronostratigraphic marker. Due to the lack of detectable volcanic glass within it, this outstanding deposition event was initially associated with sub-glacial volcanism or with volcanic activity outside the Antarctic continent (Hammer et al., 1997); more recently an Antarctic source has been inferred (Vallelonga et al., 2005). Our study documents the first finding of discrete tephra within this well-known event. Perhaps this tephra and the exceptionally long-lasting gaseous emission have originated from the same source; however, from the observed stratigraphic concomitance alone it is difficult to definitely assess a genetic relationship between the two. Notwithstanding, the TD822 position within the distinctive stratigraphic event adds value of this

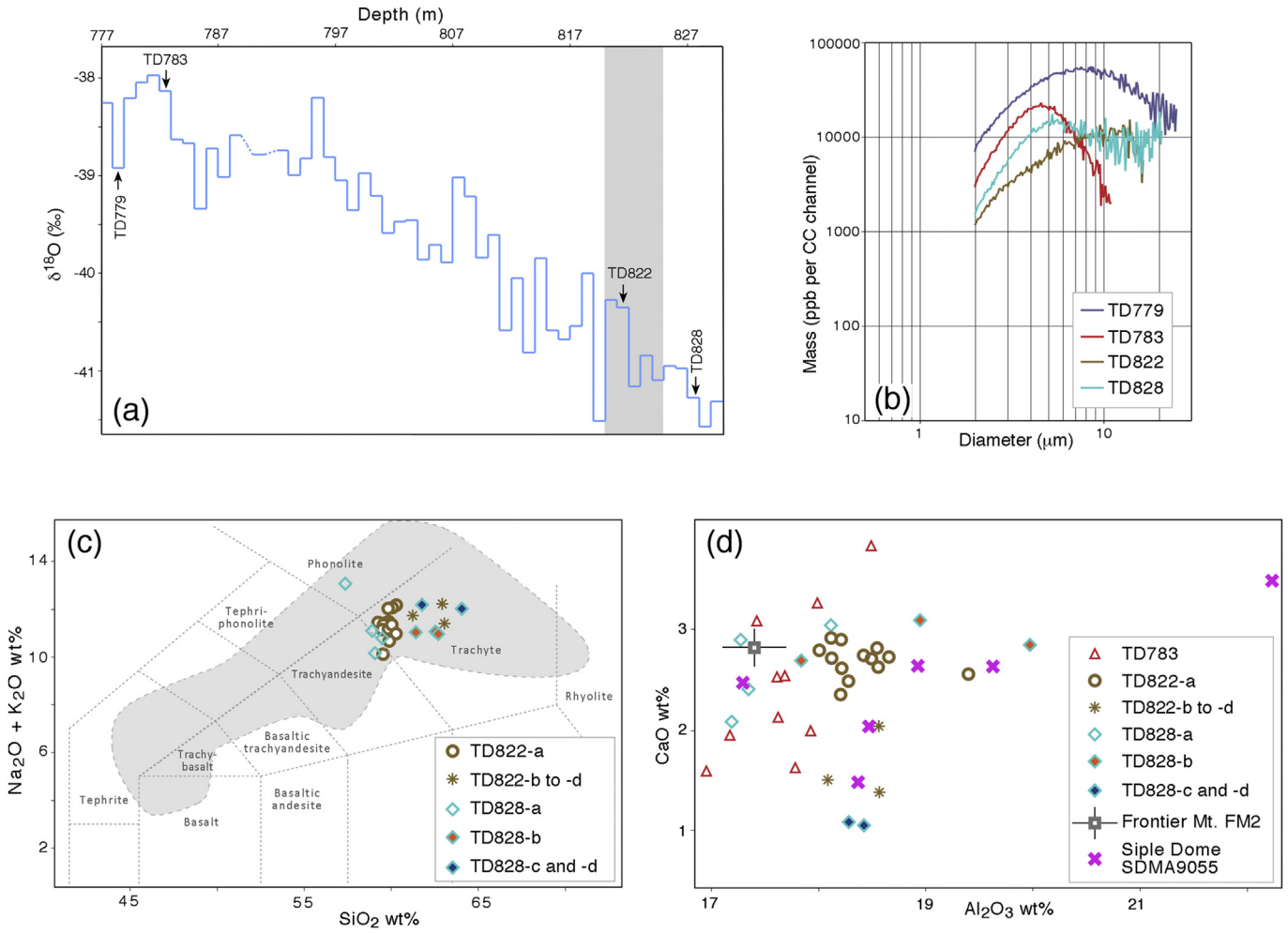

Fig. 3. Details of tephras located in the last deglaciation core sections. (a) Climate ($\delta^{18}O$) record vs. depth showing the stratigraphic position of tephra layers (TD779 and TD783 layers were reported by Narcisi et al., 2012). Shading indicates the position of the 'fluoride main event'. (b) Mass-size distributions of tephra samples obtained by quantitative particle size analysis. (c) Total alkali-silica classification diagram (Rickwood, 1989, and references therein) for glass shards from the analysed tephras. Data shown are normalised values. The compositional envelope for all local tephras identified within the TALDICE ice core drawn from data from the present study and published references (Narcisi et al., 2012; Narcisi et al., 2016) is provided for comparison. (d) Biplot comparing major element compositions of tephra deposits. For details of Frontier Mt. and Siple Dome samples see the text.

tephra as isochron for future correlations.

TD828 (18.00 ± 0.82 ka) is a visually prominent dark grey layer ca. 5-mm thick and containing coarse (ca. 100 μm) vesicular particles. A total of nine microprobe analyses were collected. We identified two coexisting trachytic glass populations (TD828-a and -b, respectively) that are distinct in their Si, Ti, Fe and Mg (Fig. 3c and Table 1). Further two glass analyses (TD828-c and -d) are trachytic but plot outside the main populations (Fig. 3d).

It is noteworthy that TD822 and TD828 main glasses have comparable chemical signature and are characterised by outstandingly high values of CaO oxide contents (average 2.7 to 2.9), this compositional feature being common also to the younger ash layer TD783 (2.43 ± 0.73 wt %, Narcisi et al., 2012) (Fig. 3d). Interestingly, a trachytic ash layer with this distinctive geochemistry was found also in the tephra succession exposed at Frontier Mountain, ca. 30 km SE from Talos Dome (sample FM2, Curzio et al., 2008) and farther away in the West Antarctic Siple Dome A ice core (sample SDMA9055, size 20 μm, 18.25 ka, Dunbar and Kurbatov, 2011), ca. 1500 km from Talos Dome (Fig. 3d). The former is a blue ice sequence containing several tens of tephra layers from Northern Victoria Land volcanoes, a few of which were already correlated with Holocene TALDICE layers (Narcisi et al., 2012). The latter is a ca. 120-ka ice-core record dominated by volcanic input from Marie Byrd Land but also with some layers from Northern Victoria Land sources. Given the chemical similarity and coherent chronostratigraphic position, we propose a one-to-one link among the tephra in blue ice, the Siple Dome tephra and TD828. Decreasing particle size of ash from Talos Dome (ca. 100 μm) to the West Antarctic Siple Dome (20 μm) is consistent with derivation from a Victoria Land source. Wide tephra deposition across the Antarctic ice sheet indicates that we are dealing with a significantly large explosive eruption that likely involved also the Ross Sea and East Pacific marine regions. Unfortunately, no marine tephra records with sufficiently resolved chronologies are yet available.

In the Last Glacial Maximum, the invisible tephra horizon TD867 (21.55 ± 1.15 ka) was identified through grain size measurements (Supplementary Table 1). This sample was not geochemically characterised by microprobe due to small grain size, however semi-quantitative EDS results from unpolished glass shards suggest an alkaline signature, consistent with rock compositions of local volcanism.

3.2.2. AIM events 3, 4 and 5

Five discrete tephra layers were identified in the core sections encompassing these warm events and related coolings (Fig. 4a). For four of them we present major element geochemistry by

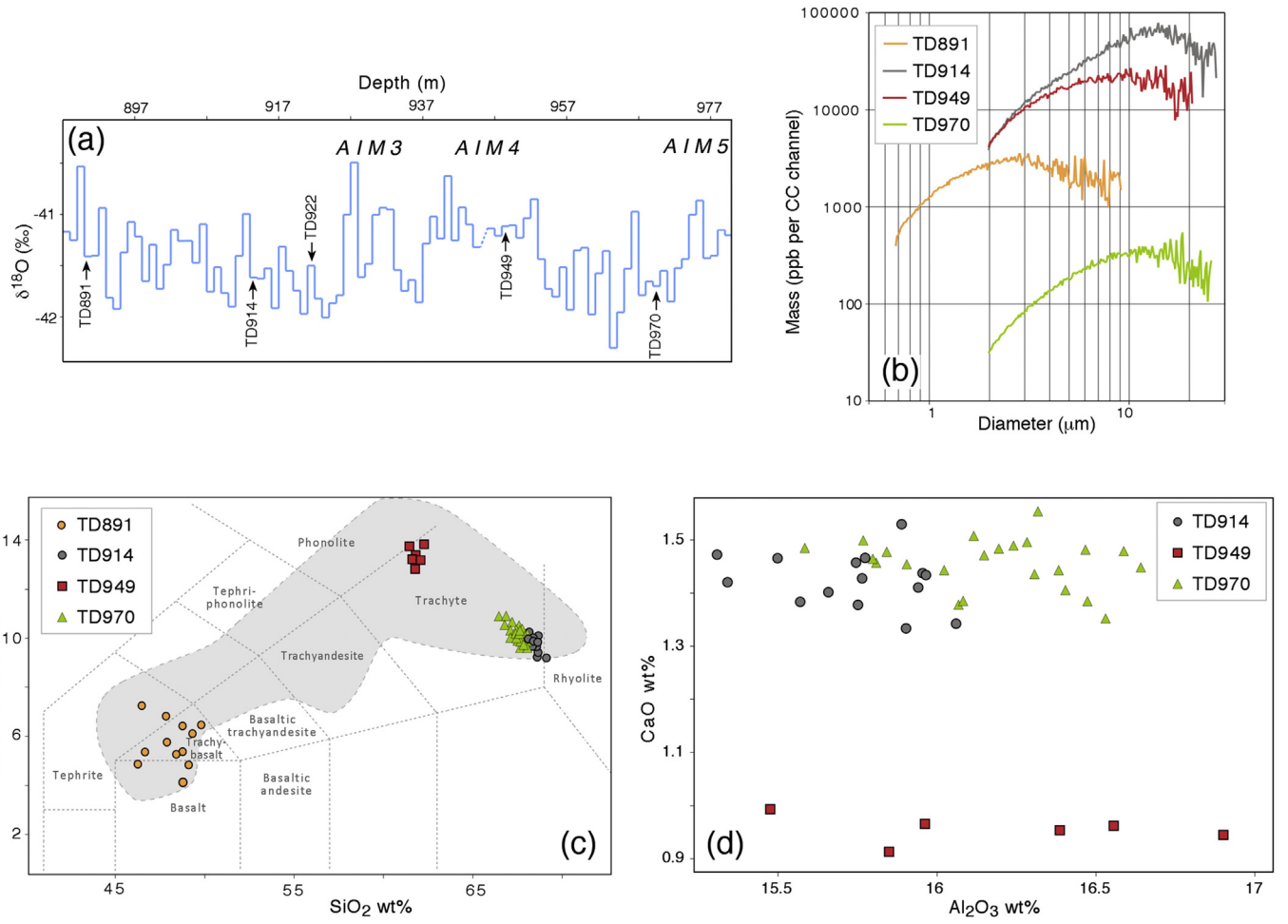

Fig. 4. Details of tephras located in the AIM 3 to AIM 5 core sections. (a) Climate ($\delta^{18}O$) record vs. depth showing the stratigraphic position of tephra layers. (b) Mass-size distributions of tephra samples obtained by quantitative particle size analysis. (c) Total alkali-silica classification diagram (Rickwood, 1989, and references therein) for glass shards from the analysed tephras. Data shown are normalised values. The compositional envelope for all local tephras identified within the TALDICE ice core drawn from data from the present study and published references (Narcisi et al., 2012; Narcisi et al., 2016) is provided for comparison. (d) Biplot comparing major element compositions of tephra deposits.

microprobe analysis (Table 1 and Fig. 4c). TD922 (27.05 ± 0.69 ka) was not examined in this study.

TD891 (23.65 ± 0.88 ka) is an invisible volcanic horizon composed of tiny glassy splinters having a maximum size of ca. 25 μm (Fig. 4b and Supplementary Fig. 2). It was deposited ca. four millennia after the culmination of Antarctic warming AIM 3 (Fig. 4a). Based on 12 major element analyses, this tephra is classified as trachybasalt (Fig. 4c).

Layers TD914 (26.16 ± 0.71 ka), TD949 (29.72 ± 0.66 ka BP), and TD970 (31.72 ± 0.66 ka) are all visually prominent and contain pumice particles up to about 80 μm in size. They are classified as trachyte, but exhibit different chemical signatures (Fig. 4c). TD949 composition falls close to the boundary with phonolite, and shows sodium enrichment (mean Na_2O/K_2O weight ratio ca. 1.85). Glasses from both TD914 and TD970 are homogeneous, and displays mean Na_2O/K_2O weight ratio ca. 0.9. They have overlapping composition considering analytical errors (Fig. 4d). Fortunately, these layers settled over five millennia apart and exhibit very distinct position relative to the rapid climate fluctuations (Fig. 4a). They therefore can be discriminated from one another using stratigraphy.

3.2.3. AIM event 8

Several discrete volcanic ash layers were identified in the ice portion recording the isotopic signal of warm event AIM 8 (Fig. 5a). Two of them (TD1042 and TD1058) are faint horizons showing similar grain size features, both as mode and concentrations (Fig. 5b). TD1042 (37.94 ± 0.49 ka) contains platy and curved vitric shards. The minute particle size (~15 μm) hampered microprobe geochemical analysis.

TD1050 is 5-mm faint horizon dated to 38.45 ± 0.48 ka. The coarsest glass particles are represented by pumice with elongated vesicles (Supplementary Fig. 2). Five shards exhibit a homogeneous trachydacitic composition (Fig. 5c).

TD1058 (38.96 ± 0.48 ka) is a 2-mm thick diffuse layer composed of glass particles up to 50 μm large, with ovoid vesicles. Four analyses indicate a rather heterogeneous trachytic composition of glass (Fig. 5c).

The ca. 4-cm thick brownish layer TD1059 (39.03 ± 0.48 ka) comprises several horizons (Supplementary Fig. 1). From the bottom part of this layer a couplet of horizons separated by 1-mm of clear ice, (Top, 7 mm thick; Bottom, 4 mm thick), were sub-sampled for this work. The material is composed of moderately vesicular glass and alkali feldspar grains. Both samples are classified as trachyte (Fig. 5c). Since they show similar composition, we suggest they could originate from two closely timed explosions of the same eruption. TD1058 and TD1059 tephras are located very closely to each other within the isotope stratigraphic record (Fig. 5a), but can be distinguished using their alumina contents (Fig. 5d).

TD1067 (39.56 ± 0.50 ka) falls at the rising slope of AIM event 8 (Fig. 5a). It is a ca. 10-cm thick layer that was readily detected due to

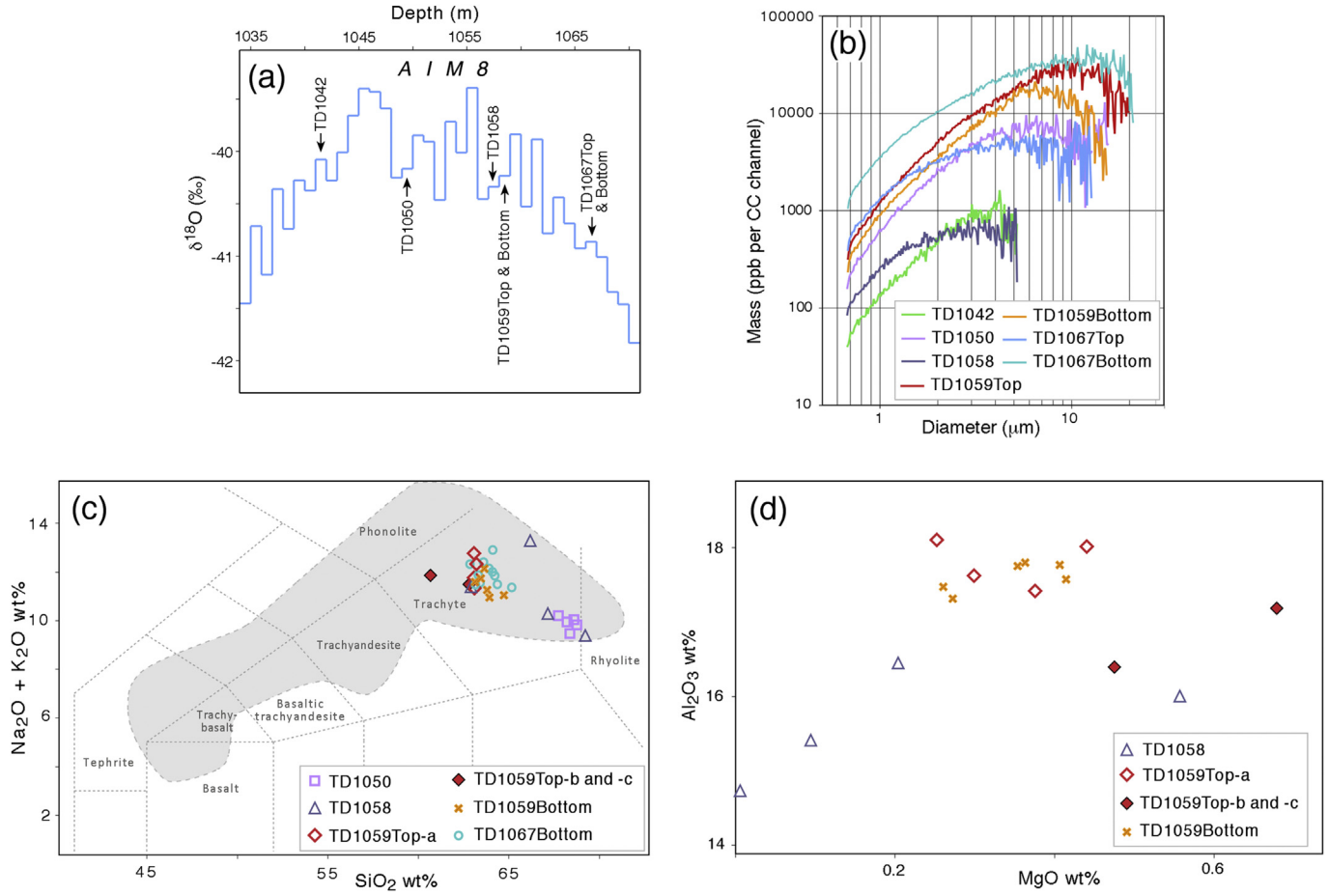

Fig. 5. Details of tephras located in the AIM 8 core sections. (a) Climate ($\delta^{18}O$) record vs. depth showing the stratigraphic position of tephra layers. (b) Mass-size distributions of tephra samples obtained by quantitative particle size analysis. (c) Total alkali-silica classification diagram (Rickwood, 1989, and references therein) for glass shards from the analysed tephras. Data shown are normalised values. The compositional envelope for all local tephras identified within the TALDICE ice core drawn from data from the present study and published references (Narcisi et al., 2012; Narcisi et al., 2016) is provided for comparison. (d) Biplot comparing major element compositions of tephra deposits.

its prominent macroscopic features (Supplementary Fig. 1). In particular, it shows a basal 2 cm dark brown band (TD1067Bottom) sharply contrasting with the underlying ice and characterised by the highest tephra fallout measured in the record (Supplementary Table 1). This ash and the sample from the upper part of the layer (TD1067Top) are composed of glass splinters that sometimes appear to be remnants of thick bubble walls, and free feldspar crystals. Microprobe measurements of eleven glass shards from TD1067Bottom indicate a homogeneous trachytic composition similar to TD1059 (Fig. 5c), however the two layers can be discriminated based on their different position with respect to the stable isotope signal (Fig. 5a).

3.2.4. AIM event 11

TD1099 (42.00 ± 0.51 ka) is stratigraphically located at the temperature minimum between events AIM 10 and AIM 11 (Fig. 6a). It is a pale visible horizon rich in alkali feldspar crystals and dense to moderately vesicular shards ca. 60 μm in size (Supplementary Fig. 2). Four microprobe analyses define a rather heterogeneous trachytic composition (Fig. 6d). A few further faint horizons occurring around TD1099 could not be sub-sampled for characterisation study.

During the cooling interval following the AIM 11 climatic event, between ca. 1104.70 and 1104.82 m depth, several closely spaced mm-thick layers labelled TD1105 occur (Fig. 6a). Based on accumulation rate at this depth, their deposition occurred within approximately a decade. The seven most obvious horizons, denoted A to G from top to bottom, were considered for this study and analysed for quantitative grain size. The lowermost studied layer (TD1105G) is the most visually evident (Supplementary Fig. 1) and is also the most concentrated (Fig. 6c). Glass shards in these layers are dense or moderately vesicular up to 50 μm in size and show spherical bubbles (Supplementary Fig. 2). Three samples from this set (C, D and G) were fingerprinted by microprobe, with a total of 52 major element analyses that mainly plot in the trachybasalt field (Fig. 6d). Thirteen different glass shards from TD1105G were analysed for their trace element contents (Supplementary Table 3 and Fig. 10). The three samples analysed by microprobe appear indistinguishable from one another (see also Fig. 6e). Given the very short time separation and the observed affinities in grain size, ash texture and geochemical composition, these layers are interpreted as related to pulses of the same explosive event.

TD1132 (44.92 ± 0.52 ka) is ca. 2 cm-thick visible layer lying stratigraphically at the temperature minimum between AIM 11 and AIM 12 (Fig. 6a). It is composed of two distinct horizons (denoted as Top and Bottom, respectively) that contain glass shards ca. 20 μm in size. Due to the limited grain size, quantitative major element analysis was not performed, however EDS spectra taken from unpolished particles suggest an alkaline evolved composition.

3.2.5. AIM event 12

Macroscopic tephra layers TD1163 and TD1164 occur at the

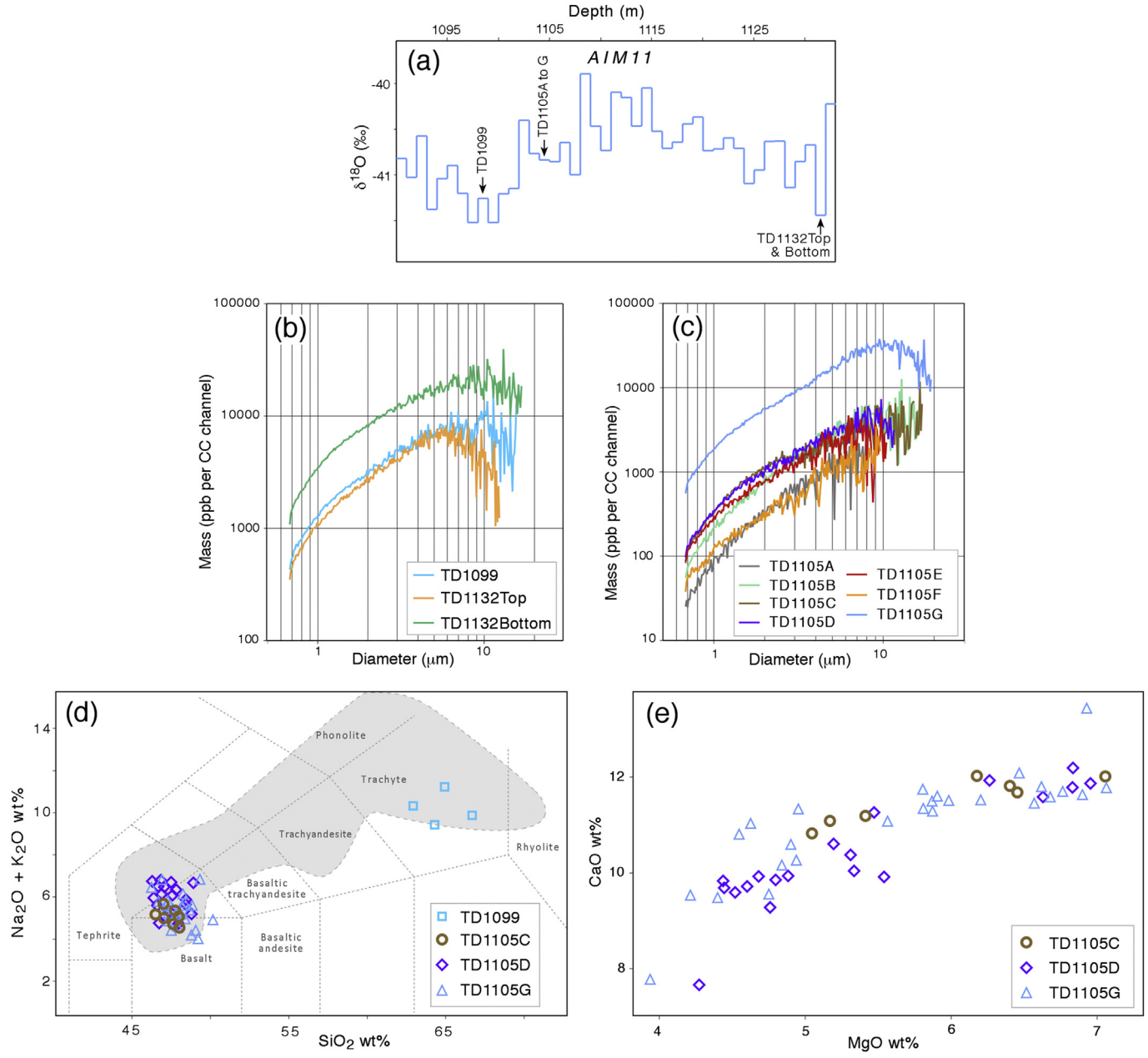

Fig. 6. Details of tephras located in the AIM 11 core sections. (a) Climate ($\delta^{18}O$) record vs. depth showing the stratigraphic position of tephra layers. (b) and (c) Mass-size distributions of tephra samples obtained by quantitative particle size analysis. (d) Total alkali-silica classification diagram (Rickwood, 1989, and references therein) for glass shards from the analysed tephras. Data shown are normalised values. The compositional envelope for all local tephras identified within the TALDICE ice core drawn from data from the present study and published references (Narcisi et al., 2012; Narcisi et al., 2016) is provided for comparison. (e) Biplot comparing major element compositions of tephra deposits.

rising thermal slope of AIM 12 (Fig. 7a) and are dated 47.20 ± 0.52 and 47.28 ± 0.60 ka, respectively. In both layers glass is represented by vesicular particles (Supplementary Fig. 2). From CC measurements, TD1163 is the coarsest of the two (Fig. 7b). Although the two layers were deposited approximately one century apart, and both are classified as trachyte (Fig. 7c), they exhibit different chemical signatures, particularly with respect to SiO_2, TiO_2, Al_2O_3, MgO and the Na_2O/K_2O ratio (Table 1). Trace element analysis that could further distinguish between the two glasses, was possible only of TD1163 (Supplementary Table 3 and Fig. 10). The observed significant differences in chemical characteristics indicate that TD1163 and TD1164 are not genetically related and likely originated from two different volcanoes within the Northern Victoria Land province.

3.2.6. AIM event 13

Five macroscopic tephra layers, labelled TD1180 (48.93 ± 0.70 ka), TD1183 (49.30 ± 0.72 ka), TD1189 (50.02 ± 0.81 ka), TD1191 (50.27 ± 0.86 ka) and TD1197 (51.04 ± 0.90 ka), respectively, are stratigraphically framed within this warming event and adjacent cool phases (Fig. 7a). Based on AICC2012, their deposition occurred within a time interval of about two millennia. Within this tephra set, two layers display basic to intermediate compositions. In particular, TD1191, made up of glass fragments up to 60 μm in size, is geochemically heterogeneous, ranging from trachyandesite to tephri-phonolite (Fig. 7d). TD1189, composed of dense to moderately vesicular glass shards, has a homogeneous basaltic composition with characteristic low K_2O contents (average ca. 1%) (Fig. 7d and Table 1). It represents the most basic tephra of local derivation

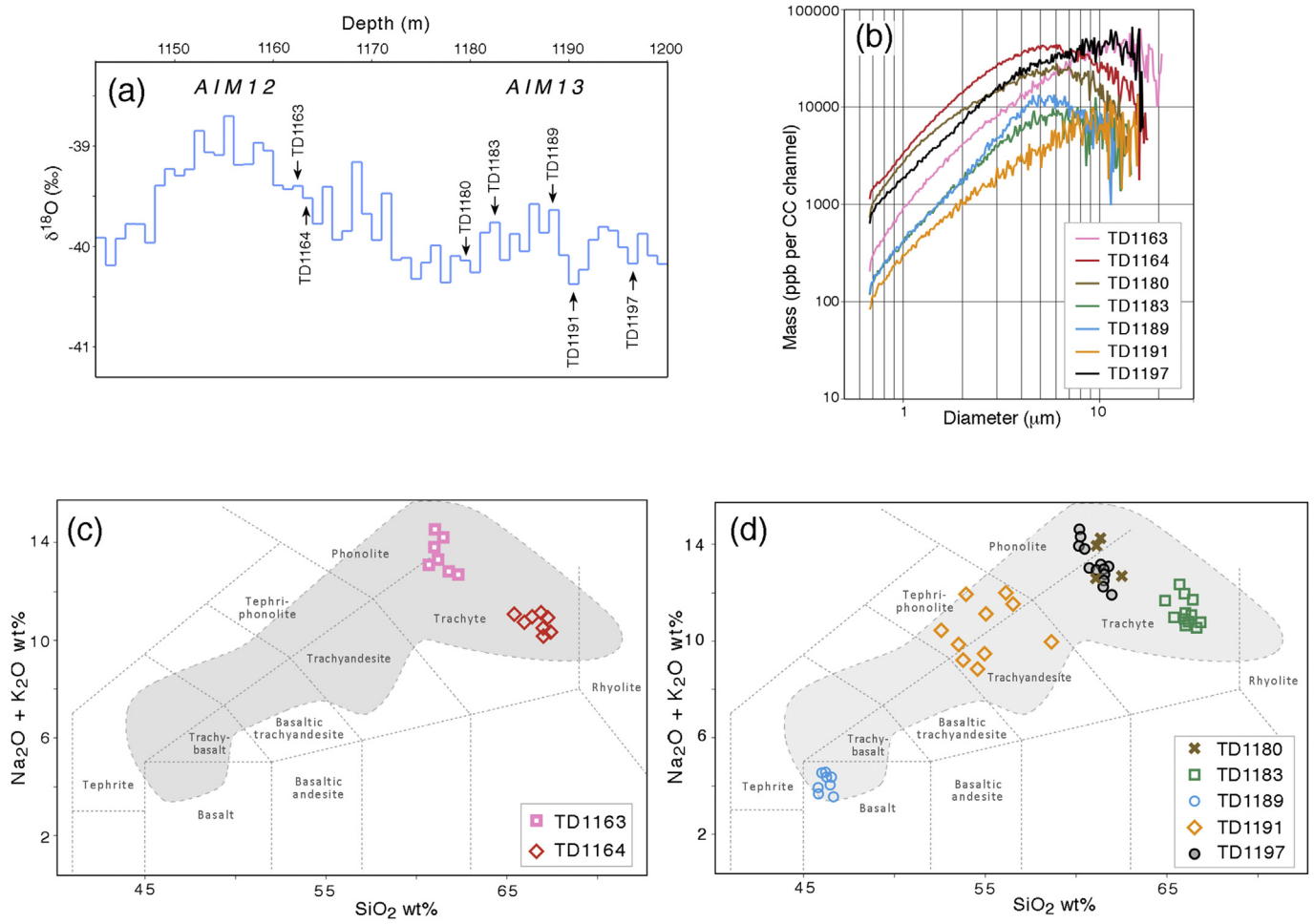

Fig. 7. Details of tephras located in the AIM 12 and AIM 13 core sections. (a) Climate ($\delta^{18}O$) record vs. depth showing the stratigraphic position of tephra layers. (b) Mass-size distributions of tephra samples obtained by quantitative particle size analysis. (c) and (d) Total alkali-silica classification diagram (Rickwood, 1989, and references therein) for glass shards from the analysed tephras. Data shown are normalised values. The compositional envelope for all local tephras identified within the TALDICE ice core drawn from data from the present study and published references (Narcisi et al., 2012; Narcisi et al., 2016) is provided for comparison.

hitherto discovered within the TALDICE ice core (c.f., Narcisi et al., 2012, 2016). Given this distinctive composition (see also Supplementary Table 3 and Fig. 10 for the trace element signature) along with its peculiar stratigraphic position at the culmination of the Antarctic warming event (Fig. 7a), this layer forms a key marker for correlation of Antarctic palaeorecords.

The three remaining layers detected in this climatic interval are trachytic (Fig. 7d). TD1180 and TD1183, deposited approximately 350 years apart, are easily distinguishable from each other by their SiO_2, Al_2O_3 and total alkali contents (Fig. 7d). TD1180 and TD1183 trace element compositions are also different and reinforce the chemical discrimination between the two tephras (Supplementary Table 3 and Fig. 10). TD1197 is chemically very similar to TD1180 (Fig. 7d). Fortunately, these two horizons, placed ca. 2000 years apart, display different position relative to the climate isotopic signal, as TD1197 deposited prior to AIM 13 warming while TD1180 occurs at the end of this event (Fig. 7a). Their different stratigraphic position therefore provides an effective criterion for tephra discrimination.

3.2.7. AIM event 14

Three volcanic horizons were recognised in the core sections recording AIM 14 (Fig. 8a).

At 52.43 ± 0.83 ka, approximately 1.8 ka after the culmination of this climatic event, two mm-thick adjacent horizons (TD1208 Top and Bottom, respectively) were identified. The material is composed of vesicular glass and according to CC measurements and microscopic observations, the Bottom horizon is coarser and more concentrated than the Top one (Fig. 8b). As for geochemistry, both samples fall in the trachytic field at the boundary with phonolite (Fig. 8c) and are rather heterogeneous (Fig. 8d). Inherent heterogeneity of this material is also observable in the trace element composition of TD1208 Top sample (Fig. 10). Given the overlapping chemical composition and the very close spacing, the two TD1208 horizons most probably represent tephra-producing explosions within the same volcanic event. The observed grading within the deposit likely reflects the decreasing intensity of the explosive eruption.

The TD1226 ash layer is dated 54.76 ± 0.7 ka and occurs ca. five centuries prior to occurrence of thermal peak related to AIM event 14 (Fig. 8a). This tephra contains coarse vesiculated pumice up to 100 μm in size and considerable amount of alkali feldspar crystals. The dominant glass (TD1226-a) is trachytic in composition (Fig. 8c). Three trachytic outliers (TD1226-b to -d) have a different signature with respect to main shard population (mean Al_2O_3 ca. 11.5%; mean FeO ca. 9.5%; Table 1). This subordinate outlier composition is inconsistent with known Victoria Land rock geochemistry, and is more similar to trachytic products from Marie Byrd Land in West Antarctica (e.g. Dunbar et al., 2008). The significance of these glass shards within the TALDICE horizon remains unclear.

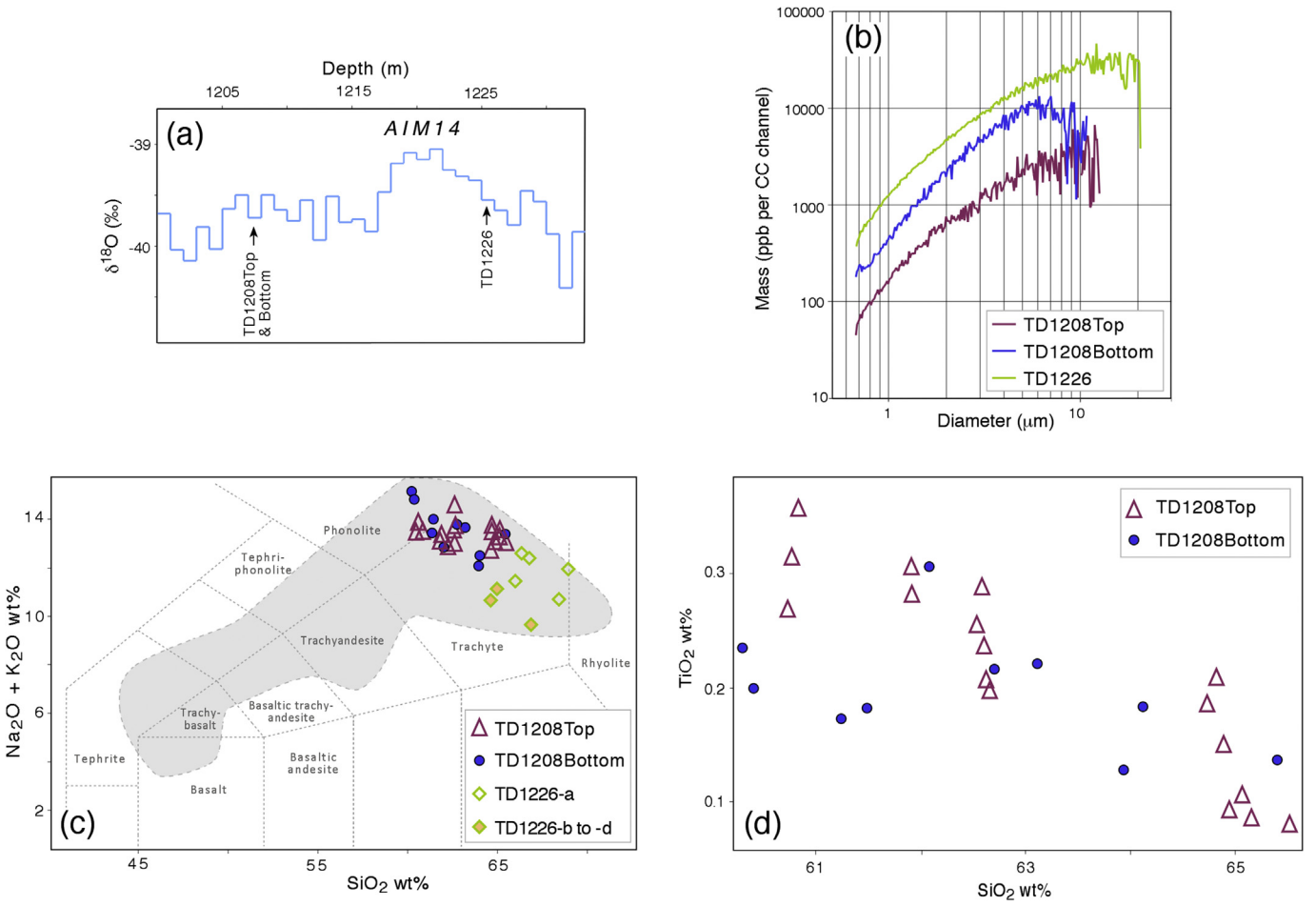

Fig. 8. Details of tephras located in the AIM 14 core sections. (a) Climate ($\delta^{18}O$) record vs. depth showing the stratigraphic position of tephra layers. (b) Mass-size distributions of tephra samples obtained by quantitative particle size analysis. (c) Total alkali-silica classification diagram (Rickwood, 1989, and references therein) for glass shards from the analysed tephras. Data shown are normalised values. The compositional envelope for all local tephras identified within the TALDICE ice core drawn from data from the present study and published references (Narcisi et al., 2012; Narcisi et al., 2016) is provided for comparison. (d) Biplot comparing major element compositions of tephra deposits.

3.2.8. AIM event 17

A total of eight discrete tephra layers were identified within the ice-core record of the prominent AIM event 17 and adjacent cooling phases (Fig. 9a). The youngest of these, labelled TD1246, is dated at 57.77 ± 0.95 ka. This sample, containing pumiceous particles with ovoid to elongated bubbles (Supplementary Fig. 2), was analysed for both major and trace element compositions (Figs. 9d and 10). 9 shards analysed by electron microprobe form the main glass population (TD1246-a) that in the TAS grid is classified as rhyolite (mean SiO_2 ca. 69.6%; mean total alkali ca. 10.4%). Two less evolved outliers (TD1246-b and -c) feature trachyte. The TD1246 main glass represents the most silicic tephra of unambiguous local derivation identified in the core thus far. By virtue of its distinctive chemistry along with its precise stratigraphic position relative to the palaeoclimatic record, this tephra could act as effective stratigraphic marker for future correlations.

Macroscopic layers TD1257 (59.40 ± 1.15 ka) and TD1258 (59.55 ± 1.17 ka) lie stratigraphically at the culmination of AIM 17 (Fig. 9a) and according to the AICC2012 were deposited approximately 150 years apart. Both samples are composed of pumiceous particles 60–70 μm in size and are chemically rather heterogeneous (Fig. 9d). Main glass composition of TD1257 (TD1257-a) is trachytic; additional three outliers are phonolitic (TD1257-b) and trachytic (TD1257-c and -d) in composition. TD1258 main glass (TD1258-a) is also trachytic, with two glass shards (TD1258-b and -c) showing outlying values for CaO (Table 1). Despite presenting narrow ages and stratigraphic position as well as similar heterogeneous character, these two layers can be readily discriminated using SiO_2 contents (Fig. 9d).

Five ash horizons were detected in the ice-core section recording the cool phase that precedes AIM 17 (Fig. 9a). Their deposition occurred within a half millennium period.

Visible layer TD1278 (63.35 ± 1.45 ka), containing coarse pumice with elongated parallel vesicles with well-preserved thin walls (Supplementary Fig. 2), was analysed for both major and trace elements (Figs. 9 and 10). It is composed of trachytic glass with mean CaO oxide ca. 0.9 wt % (Table 1).

Three visually distinct horizons dated at 63.61 ± 1.44 ka occur within the narrow core section between 1278.49 and 1278.51 m depth (Fig. 9a). These TD1279 layers, denoted A to C from top to bottom, were deposited within a few year period. The samples contain pumice particles and free alkali feldspar crystals. Both CC granulometric measurements and microscopic observations indicate progressive decrease of grain size and amount of ash fallout from C to A samples (Fig. 9c and Supplementary Table 1). Glasses from this triplet are chemically similar in that they display remarkable internal variation (Fig. 9e). Four individual shards from TD1279A feature tephrite, basaltic trachyandesite and trachyandesite, respectively. The main glass population from TD1279B (TD1279B-a) is trachytic, but with one glass shard (TD1279B-b)

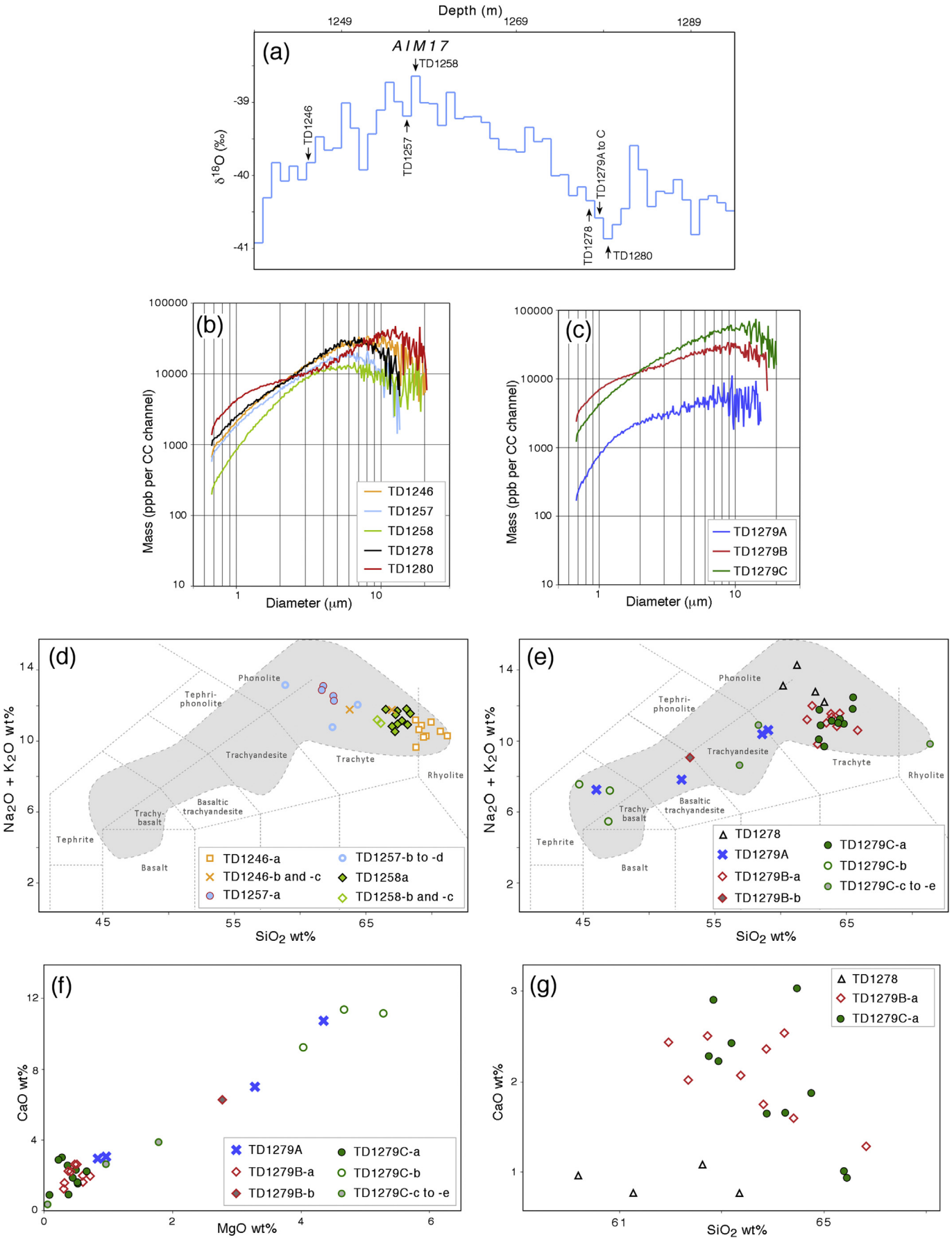
(a)
AIM17
Depth (m)
1249
1269
1289
TD1258
TD1246
TD1257
TD1279A to C
TD1278
TD1280
δ18O (‰)
-39
-40
-41
(b)
Mass (ppb per CC channel)
Diameter (μm)
TD1246
TD1257
TD1258
TD1278
TD1280
(c)
TD1279A
TD1279B
TD1279C
(d)
Na2O + K2O wt%
SiO2 wt%
Phonolite
Tephri-phonolite
Trachyandesite
Trachyte
Rhyolite
Basaltic trachyandesite
Trachy-basalt
Tephrite
Basalt
TD1246-a
TD1246-b and -c
TD1257-a
TD1257-b to -d
TD1258a
TD1258-b and -c
(e)
TD1278
TD1279A
TD1279B-a
TD1279B-b
TD1279C-a
TD1279C-b
TD1279C-c to -e
(f)
CaO wt%
MgO wt%
(g)
SiO2 wt%

featuring basaltic trachyandesite. TD1279C contains a dominant glass population of trachytic composition (TD1279C-a), a tephritic glass subset (TD1279C-b) and further three shards (TD1279C-c to -e) that are trachyandesitic and rhyolitic, respectively. Interestingly, taken as a whole the multiple glass compositions from these samples appear arranged along a coherent magmatic fractionation trend (Fig. 9f), suggesting that they are genetically related. Likely, they represent different pulses of a single eruption from a compositionally zoned magma body. Normal grading indicates decreasing eruption intensity versus time. We point out that compositional heterogeneity inside Talos Dome ash layers is not uncommon, and identical fractionation trend lines were observed in some Holocene layers attributed to Mt. Melbourne volcano (Narcisi et al., 2012). Despite presenting very close stratigraphic location within the isotopic record and temporal separation of approximately 250 years, trachytic tephra TD1278 and the trachytic glass populations TD1279B-a and TD1279C-a inside TD1279 layers can be discriminated based on their different CaO contents (Fig. 9g).

The lowermost identified layer, TD1280 (63.87 ± 1.44 ka), is visually prominent (Supplementary Fig. 1) and displays bimodal size distribution (Fig. 9b). The material, composed of pumice and shards up to ca. 60 μm in size, was not analysed with WDS microprobe, however semi-quantitative chemical analysis of unpolished particles indicates an alkali-trachytic signature.

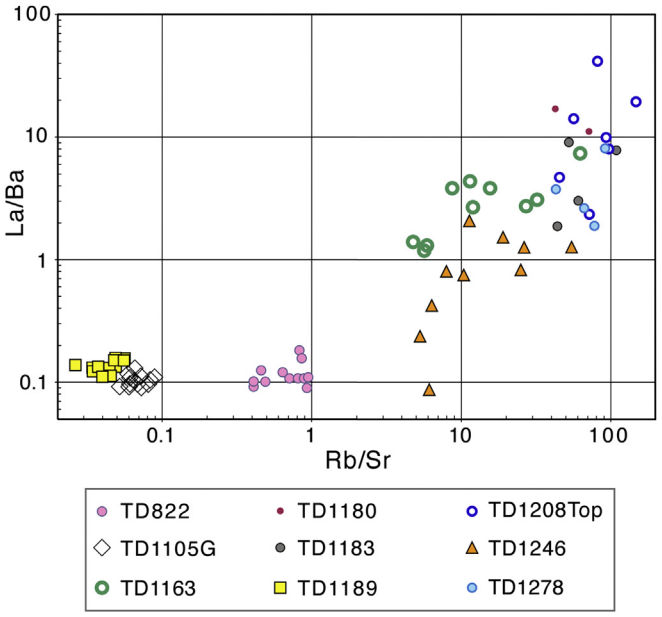

Fig. 10. Trace element compositional plot on a bilogarithmic scale portraying the signature of individual glass shards. Circular symbols indicate samples with trachytic major element chemistry.

4. Implications and summary

The TALDICE tephra sequence includes traces of about forty separate explosive eruptions that occurred between ca. 17.6 and ca. 64 ka. All studied layers are derived from primary deposition. They were geochemically fingerprinted and robustly constrained from age and stratigraphy points of views. The developed record, far from being a simple compilation of a tephra dataset, can be regarded as a reference East Antarctic tephrostratigraphy upon which robust stratigraphic correlations and palaeovolcanic reconstructions can be reliably based.

Concerning our stratigraphic purpose, we point out that the tephra record is dominated by volcanic input from a single source area, and the samples therefore share a common petrological character (Fig. 2). As in other case studies influenced by high-frequency tephra deposition from a major volcanic contributor (e.g. Bourne et al., 2015) similar geochemical compositions could in principle complicate and even hinder the usage of individual tephra horizons for accurate correlations (Smellie, 1999; Hillenbrand et al., 2008). We have shown, however, that the TALDICE layers can be reliably distinguished from one another using subtle but significant differences in geochemical major element compositions and trace elements as additional fingerprint. In addition, a few studied layers (e.g. TD822, TD828, TD1189, TD1246) are geochemically very distinctive and therefore represent reliable markers for future identification in other palaeo-archives. Most importantly, each studied layer is precisely positioned within the dated palaeoclimate record. The stratigraphic criterion appears to be of crucial importance to make distinction between tephra with similar signatures but with different position with respect to climate signals. Among identified markers, the TD822 ash horizon settled at ca. 17.6 ka during deposition of the well-known acidity peak provides a standout stratigraphic tie-point. To date this is the only documented occurrence of volcanic glass within this continentally-significant event. Also, we have proposed the correlation between TD828 and a volcanic horizon detected in a West Antarctic ice core. A few cases of widespread correlations of TALDICE tephras deposited during the last glacial-interglacial climatic cycle are already available (see also Narcisi et al., 2012). We expect that the regional tephrostratigraphic scheme will widen, involving not only Antarctic ice sheet sites but also the marine region facing the Victoria Land, once new detailed sediment records containing tephra layers will be compiled. In fact, physical properties of several TALDICE layers (considerable thickness and tephra fallout, coarse size and high vesicularity of glass shards) strongly suggest derivation from high-energetic eruptions capable of dispersing solid material over vast areas. Note that the use of tephra isochrons for correlation could circumvent the typical issues associated with dating of sediments from high latitude regions (Cao et al., 2007; Hall et al., 2010), also considering that some climatic events of the last glacial are around or beyond the limit of radiocarbon method. This allows the findings presented in this study to be placed within a broader context. Precise, direct linkage of ice-sediment palaeorecords through tephra markers could be important to obtain a better climate and environmental perspective at continental and regional scales.

The other objective of this study is to contribute to the regional eruption record. Tephra sequences preserved in distal settings can yield important information on past explosive volcanism, especially in cases of remote inaccessible volcanoes, and when proximal products are buried by ice cover or by subsequent deposits (Dunbar et al., 2008; Iverson et al., 2014). The TALDICE tephra archive is central in this respect, considering that the chrono-stratigraphy and geochemistry of the Antarctic North Victoria Land volcanoes are incompletely characterised. The limited surficial information

Fig. 9. Details of tephras located in the AIM 17 core sections. (a) Climate ($\delta^{18}O$) record vs. depth showing the stratigraphic position of tephra layers. (b) and (c) Mass-size distributions of tephra samples obtained by quantitative particle size analysis. (d) and (e) Total alkali-silica classification diagram (Rickwood, 1989, and references therein) for glass shards from the analysed tephras. Data shown are normalised values. The compositional envelope for all local tephras identified within the TALDICE ice core drawn from data from the present study and published references (Narcisi et al., 2012; Narcisi et al., 2016) is provided for comparison. (f) and (g) Biplots comparing major element compositions of tephra deposits.

for The Pleiades and Mt. Rittmann sources suggests that they were active during the Upper Pleistocene until likely historical times, however very few radiometric dates are available, and these were obtained exclusively on lava flows (Kyle, 1982; Perchiazzi et al., 1999). The stratigraphic evolution of Mt. Melbourne during the last glacial-interglacial climatic cycle is better characterised (Giordano et al., 2012), but the published age measurements for products within the glacial period are very imprecise. Our continuous tephra series provides an unparalleled means for accurate volcanic reconstruction as each fingerprinted layer documents a highly time-constrained, previously undefined explosive eruption.

Occurrence of multiple closely-spaced tephra horizons in the study core demonstrates strong persistent explosive activity in the source area during the studied glacial times. Within this general behaviour, a few ice sections related to millennial-long intervals (e.g. ca. 32 to 38 ka; ca. 55 to 58 ka; ca. 64 to 71 ka, age of bottom of the investigated core sections) do not hold discrete tephras (Fig. 1b). These intervals could be interpreted as dormant periods. However, some caution is required at this stage considering that the presented volcanic record, based mainly on macroscopic ash layers, could lack lower-intensity explosive eruptions and also evidently do not include traces of purely effusive activity. Likewise, although we are aware of the interest in investigating possible response of Antarctic volcanism to climate variations (e.g. Nyland et al., 2013), limitations to obtaining an exhaustive volcanic record suggest us to refrain from deriving quantitative changes of the eruption frequency from the presented tephrostratigraphy.

Our findings could also offer new insight into temporal geochemical variations. For this purpose, we have compared volcanic glass analytical results with prior compositional data for TALDICE tephras deposited during the last and present interglacials (Fig. 11). Thirteen tephra layers dated between ca. 123 and 112 ka (±ca. 2 ka) were identified and characterised in the core interval related to Eemian and the transition to the subsequent glacial period (Narcisi et al., 2016). Seventeen local tephra events were detected in the postglacial period between 15.5 and 0.7 ka (Narcisi et al., 2012).

First, we observe that the single glass-shard data taken as a whole define a continuous fractionation trend with time (Fig. 11). This is somewhat different from the published pattern based on whole-rock analyses (Fig. 2a). Data for Mt. Rittmann and Melbourne volcanoes (Armienti and Tripodo, 1991; Giordano et al., 2012) suggest a gap of intermediate compositions (trachyandesites), but these are observed in the TALDICE volcanic sequence. This demonstrates that unlike bulk chemistry of proximal samples, our grain-specific approach applied to distal deposits is capable of capturing a wider spectrum of composition as well as to unravel complex geochemistries inside single horizons. Secondly, we observe that the Eemian period (123-112 ka) is dominated by deposition of trachytic tephras (SiO_2 ca. 60–67 wt %). During the glacial period investigated here, trachytes are still significantly represented but appear less abundant than in the older time window. Products with intermediate and basic (e.g. trachybasalt) compositions are also observed. In the interval spanning the last 15 ka, fewer trachytic tephras are observed with respect to the older considered periods. Although quantitative estimates for the volumes of the erupted materials should also be taken into account, the tephra data suggest a general temporal shift of the regional volcanism towards less evolved compositions, similarly to what observed in other Antarctic volcanoes (e.g. Dunbar et al., 2008). Note the consequences of our temporal geochemical reconstruction also for future chronostratigraphic correlations. A newly identified tephra with no age control showing intermediate composition cannot have been erupted during the Eemian interglacial.

In summary, the TALDICE core, strategically located with respect to Northern Victoria Land source vents, preserves a high temporal resolution record of regionally significant volcanic eruptions. Through a detailed multi-parameter characterisation of individual tephra layers, and taking advantage of the completeness of the ice sequence and of its well-constrained chronostratigraphy, we have provided a wealth of last glacial tie-points for future extensive correlations of climate records. By integrating present results with previous work, the TALDICE inventory already consists of several tens of dated tephra deposits emplaced during the last glacial-interglacial cycle and represents therefore a fundamental complement of the proximal record to enhance knowledge of the volcanic history. Our study has provided evidence that the Northern Victoria Land volcanoes, presently in a quiescent state, have been more active than previously recognised from field studies. Ice-core findings for explosive frequency and temporal trends in fallout product composition could have wider interest for the assessment of volcanic hazard from future eruptions, which is still poorly understood at these volcanoes.

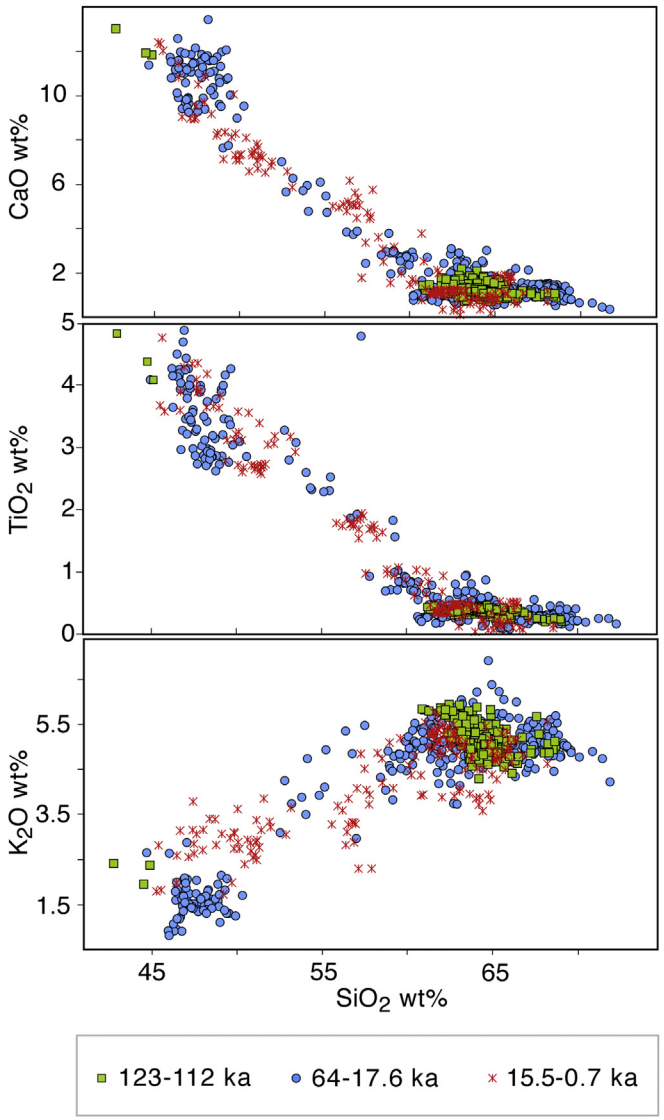

Fig. 11. Selected Harker diagrams comparing the TALDICE tephra composition for layers examined in this study (64–17.6 ka) with those identified in the Eemian (123–112 ka, Narcisi et al., 2016) and in postglacial core sections (15.5–0.7 ka, Narcisi et al., 2012). All shown data are single glass shard analyses normalised to 100%.

Acknowledgements

TALos Dome Ice CorE (TALDICE) is a joint European programme lead by Italy and funded by national contributions from Italy, France, Germany, Switzerland and the United Kingdom. This work was funded by the Italian Programma Nazionale di Ricerche in Antartide (PNRA). We thank the logistic and drilling TALDICE team, M. Tonelli (CIGS, Modena) and R. Carampin (CNR, Padova) for assistance during microanalytical work, J. Chappellaz for diligently taking pictures of tephra layers during fieldwork, two journal reviewers for their constructive comments. This is TALDICE publication no. 47. Author contributions: B.N. conceived the study, conducted tephra analysis and data interpretation, wrote the manuscript and created the figures. J.R.P. conducted ice-core sample processing and ash recovery, performed grain-size analysis and prepared the related diagrams, and contributed to the manuscript text. A.L. conducted trace element measurements and elaborated the data.

Appendix A. Supplementary data

Supplementary data related to this article can be found at http://dx.doi.org/10.1016/j.quascirev.2017.04.025.

References

Albani, S., Delmonte, B., Maggi, V., Baroni, C., Petit, J.-R., Stenni, B., Mazzola, C., Frezzotti, M., 2012. Interpreting last glacial to Holocene dust changes at Talos Dome (East Antarctica): implications for atmospheric variations from regional to hemispheric scales. Clim. Past 8, 741–750. http://dx.doi.org/10.5194/cp-8-741-2012.

Armienti, P., Tripodo, A., 1991. Petrography and chemistry of lavas and comagmatic xenoliths of Mt Rittmann, a volcano discovered during the IV Italian expedition in Northern Victoria Land (Antarctica). Mem. Soc. Geol. Ital. 46, 427–451.

Armienti, P., Civetta, L., Innocenti, F., Manetti, P., Tripodo, A., Villari, L., Vita, G., 1991. New petrological and geochemical data on Mt. Melbourne volcanic field, Northern Victoria Land, Antarctica (II Italian antarctic expedition). Mem. Soc. Geol. Ital. 46, 397–424.

Blunier, T., Brook, E.J., 2001. Timing of millennial-scale climate change in Antarctica and Greenland during the last glacial period. Science 291, 109–112. http://dx.doi.org/10.1126/science.291.5501.109.

Bourne, A.J., Cook, E., Abbott, P.M., Seierstad, I.K., Steffensen, J.P., Svensson, A., Fischer, H., Schüpbach, S., Davies, S.M., 2015. A tephra lattice for Greenland and a reconstruction of volcanic events spanning 25-45 ka b2k. Quat. Sci. Rev. 118, 122–141. http://dx.doi.org/10.1016/j.quascirev.2014.07.017.

Buiron, D., Stenni, B., Chappellaz, J., Landais, A., Baumgartner, M., Bonazza, M., Capron, E., Frezzotti, M., Kageyama, M., Lemieux-Dudon, B., Masson-Delmotte, V., Parrenin, F., Schilt, A., Selmo, E., Severi, M., Swingedouw, D., Udisti, R., 2012. Regional imprints of millennial variability during the MIS 3 period around Antarctica. Quat. Sci. Rev. 48, 99–112. http://dx.doi.org/10.1016/j.quascirev.2012.05.023.

Cao, L., Fairbanks, R.G., Mortlock, R.A., Risk, M.J., 2007. Radiocarbon reservoir age of high latitude North Atlantic surface water during the last deglacial. Quat. Sci. Rev. 26, 732–742. http://dx.doi.org/10.1016/j.quascirev.2006.10.001.

Curzio, P., Folco, L., Laurenzi, M.A., Mellini, M., Zeoli, A., 2008. A tephra chronostratigraphic framework for the Frontier Mountain blue-ice field (Northern Victoria Land, Antarctica). Quat. Sci. Rev. 27, 602–620. http://dx.doi.org/10.1016/j.quascirev.2007.11.017.

Davies, S.M., Wastegård, S., Abbott, P.M., Barbante, C., Bigler, M., Johnsen, S.J., Rasmussen, T.L., Steffensen, J.P., Svensson, A., 2010. Tracing volcanic events in the NGRIP ice-core and synchronising North Atlantic marine records during the Last Glacial period. Earth Planet. Sci. Lett. 294, 69–79. http://dx.doi.org/10.1016/j.epsl.2010.03.004.

Del Carlo, P., Di Roberto, A., Di Vincenzo, G., Bertagnini, A., Landi, P., Pompilio, M., Colizza, E., Giordano, G., 2015. Late Pleistocene-Holocene volcanic activity in northern Victoria Land recorded in Ross Sea (Antarctica) marine sediments. Bull. Volcanol. 77, 36. http://dx.doi.org/10.1007/s00445-015-0924-0.

Delmonte, B., Petit, J.R., Maggi, V., 2002. Glacial to Holocene implications of the new 27000-year dust record from the EPICA Dome C (East Antarctica) ice core. Clim. Dyn. 18, 647–660. http://dx.doi.org/10.1007/s00382-001-0193-9.

Dunbar, N.W., Kurbatov, A.V., 2011. Tephrochronology of the Siple Dome ice core, West Antarctica: correlations and sources. Quat. Sci. Rev. 30, 1602–1614. http://dx.doi.org/10.1016/j.quascirev.2011.03.015.

Dunbar, N.W., McIntosh, W.C., Esser, R.P., 2008. Physical setting and tephrochronology of the summit caldera ice record at Moult Moulton, West Antarctica. Geol. Soc. Am. Bull. 120, 796–812. http://dx.doi.org/10.1130/B26140.1.

EPICA Community Members, 2006. One-to-one coupling of glacial climate variability in Greenland and Antarctica. Nature 444, 195–198. http://dx.doi.org/10.1038/nature05301.

Giordano, G., Lucci, F., Phillips, D., Cozzupoli, D., Runci, V., 2012. Stratigraphy, geochronology and evolution of the Mt. Melbourne volcanic field (North Victoria Land, Antarctica). Bull. Volcanol. 74, 1985–2005. http://dx.doi.org/10.1007/s00445-012-0643-8.

Hall, B.L., Henderson, G.M., Baroni, C., Kellogg, T.B., 2010. Constant Holocene Southern-Ocean ^{14}C reservoir ages and ice-shelf flow rates. Earth Planet. Sci. Lett. 296, 115–123.

Hammer, C.U., Clausen, H.B., Langway Jr., C.C., 1997. 50,000 years of recorded global volcanism. Clim. Change 35, 1–15.

Hillenbrand, C.-D., Moreton, S.G., Caburlotto, A., Pudsey, C.J., Lucchi, R.G., Smellie, J.L., Benetti, S., Grobe, H., Hunt, J.B., Larter, R.D., 2008. Volcanic time-markers for Marine Isotopic Stages 6 and 5 in Southern Ocean sediments and Antarctic ice cores: implications for tephra correlations between palaeoclimatic records. Quat. Sci. Rev. 27, 518–540. http://dx.doi.org/10.1016/j.quascirev.2007.11.009.

Iverson, N.A., Kyle, P.R., Dunbar, N.W., McIntosh, W.C., Pearce, N.J.G., 2014. Eruptive history and magmatic stability of Erebus volcano, Antarctica: insights from englacial tephra. Geochem. Geophys. Geosys. 15, 4180–4202. http://dx.doi.org/10.1002/2014GC005435.

Kyle, P.R., 1982. Volcanic geology of the Pleiades, Northern Victoria Land, Antarctica. In: Craddock, C. (Ed.), Antarctic Geoscience. The University of Wisconsin Press, Madison, pp. 747–754.

Kyle, P.R., 1986. Mineral chemistry of late Cenozoic McMurdo volcanic group rocks from the Pleiades, Northern Victoria Land. Antarct. Res. Ser. 46, 305–337.

Landais, A., Masson-Delmotte, V., Stenni, B., Selmo, E., Roche, D.M., Jouzel, J., Lambert, F., Guillevic, M., Bazin, L., Arzel, O., Vinther, B., Gkinis, V., Popp, T., 2015. A review of the bi-polar see-saw from synchonized and high resolution water stable isotope records from Greenland and East Antarctica. Quat. Sci. Rev. 114, 18–32. http://dx.doi.org/10.1016/j.quascirev.2015.01.031.

Licht, K.J., Dunbar, N.W., Andrews, J.T., Jennings, A.E., 1999. Distinguishing subglacial till and glacial marine diamictons in the western Ross Sea, Antarctica: implications for a last glacial maximum grounding line. Geol. Soc. Am. Bull. 111, 91–103.

Lowe, D.J., 2011. Tephrochronology and its application: a review. Quat. Geochronol. 6, 107–153. http://dx.doi.org/10.1016/j.quageo.2010.08.003.

Narcisi, B., Proposito, M., Frezzotti, M., 2001. Ice record of a 13th century explosive volcanic eruption in northern Victoria Land, East Antarctica. Ant. Sci. 13, 174–181.

Narcisi, B., Petit, J.R., Chappellaz, J., 2010a. A 70ka record of explosive eruptions from the TALDICE ice core (Talos Dome, East Antarctic plateau). J. Quat. Sci. 25, 844–849. http://dx.doi.org/10.1002/jqs.1427.

Narcisi, B., Petit, J.R., Delmonte, B., 2010b. Extended East Antarctic ice core tephrostratigraphy. Quat. Sci. Rev. 29, 21–27. http://dx.doi.org/10.1016/j.quascirev.2009.07.009.

Narcisi, B., Petit, J.R., Delmonte, B., Scarchilli, C., Stenni, B., 2012. A 16,000-yr tephra framework for the Antarctic ice sheet: a contribution from the new Talos Dome core. Quat. Sci. Rev. 49, 52–63. http://dx.doi.org/10.1016/j.quascirev.2012.06.011.

Narcisi, B., Petit, J.R., Langone, A., Stenni, B., 2016. A new Eemian record of Antarctic tephra layers retrieved from the Talos Dome ice core (Northern Victoria Land). Glob. Planet. Change 137, 69–78. http://dx.doi.org/10.1016/j.gloplacha.2015.12.016.

Nyland, R.E., Panter, K.S., Rocchi, S., Di Vincenzo, G., Del Carlo, P., Tiepolo, M., Field, B., Gorsevski, P., 2013. Volcanic activity and its link to glaciation cycles: single-grain age and geochemistry of Early to Middle Miocene volcanic glass from ANDRILL AND-2A core, Antarctica. J. Volcanol. Geotherm. Res. 250, 106–128. http://dx.doi.org/10.1016/j.jvolgeores.2012.11.008.

Perchiazzi, N., Folco, L., Mellini, M., 1999. Volcanic ash bands in the Frontier mountain and Lichen hills blue-ice fields, northern Victoria Land. Ant. Sci. 11, 353–361.

Ponomareva, V., Portnyagin, M., Davies, S.M., 2015. Tephra without borders: far-reaching clues into past explosive eruptions. Front. Earth Sci. 3 (83) http://dx.doi.org/10.3389/feart.2015.00083.

Rickwood, P.C., 1989. Boundary lines within petrologic diagrams which uses oxides of major and minor elements. Lithos 22, 247–263.

Robock, A., 2000. Volcanic eruptions and climate. Rev. Geophys. 38 (2), 191–219. http://dx.doi.org/10.1029/1998RG000054.

Sala, M., Delmonte, B., Frezzotti, M., Proposito, M., Scarchilli, C., Maggi, V., Artioli, G., Dapiaggi, M., Marino, F., Ricci, P.C., De Giudici, G., 2008. Evidence of calcium carbonates in coastal (Talos Dome and Ross Sea area) East Antarctica snow and firn: environmental and climatic implications. Earth Planet. Sci. Lett. 271, 43–52. http://dx.doi.org/10.1016/j.epsl.2008.03.045.

Scarchilli, C., Frezzotti, M., Ruti, P.M., 2011. Snow precipitation at four ice core sites in East Antarctica: provenance, seasonality and blocking factors. Clim. Dyn. 37, 2107–2125. http://dx.doi.org/10.1007/s00382-010-0946-4.

Schwander, J., Jouzel, J., Hammer, C.U., Petit, J.R., Udisti, R., Wolff, E., 2001. A tentative chronology for the EPICA Dome Concordia ice core. Geophys. Res. Lett. 28 (22), 4243–4246.

Sigl, M., Winstrup, M., McConnell, J.R., Welten, K.C., Plunkett, G., Ludlow, F., Büntgen, U., Caffee, M., Chellman, N., Dahl-Jensen, D., Fischer, H., Kipfstuhl, S., Kostick, C., Maselli, O.J., Mekhaldi, F., Mulvaney, R., Muscheler, R., Pasteris, D.R., Pilcher, J.R., Salzer, M., Schüpbach, S., Steffensen, J.P., Vinther, B.M.,

Woodruff, T.E., 2015. Timing and climate forcing of volcanic eruptions for the past 2,500 years. Nature 523, 543–549. http://dx.doi.org/10.1038/nature14565.
Sigl, M., Fudge, T.J., Winstrup, M., Cole-Dai, J., Ferris, D., McConnell, J.R., Taylor, K.C., Welten, K.C., Woodruff, T.E., Adolphi, F., Bisiaux, M., Brook, E.J., Buizert, C., Caffee, M.W., Dunbar, N.W., Edwards, R., Geng, L., Iverson, N., Koffman, B., Layman, L., Maselli, O.J., McGwire, K., Muscheler, R., Nishiizumi, K., Pasteris, D.R., Rhodes, R.H., Sowers, T.A., 2016. The WAIS Divide deep ice core WD2014 chronology – part 2: annual layer counting (0-31 ka BP). Clim. Past 12, 769–786. http://dx.doi.org/10.5194/cp-12-769-2016.
Smellie, J.L., 1999. The Upper Cenozoic tephra record in the south polar region: a review. Glob. Planet. Change 21, 51–70.
Stenni, B., Buiron, D., Frezzotti, M., Albani, S., Barbante, C., Bard, E., Barnola, J.M., Baroni, M., Baumgartner, M., Bonazza, M., Capron, E., Castellano, E., Chappellaz, J., Delmonte, B., Falourd, S., Genoni, L., Iacumin, P., Jouzel, J., Kipfstuhl, S., Landais, A., Lemieux-Dudon, B., Maggi, V., Masson-Delmotte, V., Mazzola, C., Minster, B., Montagnat, M., Mulvaney, R., Narcisi, B., Oerter, H., Parrenin, F., Petit, J.R., Ritz, C., Scarchilli, C., Schilt, A., Schüpbach, S., Schwander, J., Selmo, E., Severi, M., Stocker, T.F., Udisti, R., 2011. Expression of the bipolar seesaw in Antarctic climate records during the last deglaciation. Nat. Geosci. 4, 46–49. http://dx.doi.org/10.1038/NGEO1026.
Thorarinsson, S., 1981. Tephra studies and tephrochronology: a historical review with special reference to Iceland. In: Self, S., Sparks, R.S.J. (Eds.), Tephra Studies, Dordrecht, Reidel, pp. 1–12.
Vallelonga, P., Gabrielli, P., Rosman, K.J.R., Barbante, C., Boutron, C.F., 2005. A 220 kyr record of Pb isotopes at Dome C Antarctica from analyses of the EPICA ice core. Geophys. Res. Lett. 32, L01706. http://dx.doi.org/10.1029/2004GL021449.
Veres, D., Bazin, L., Landais, A., Toyé Mahamadou Kele, H., Lemieux-Dudon, B., Parrenin, F., Martinerie, P., Blayo, E., Blunier, T., Capron, E., Chappellaz, J., Rasmussen, S.O., Severi, M., Svensson, A., Vinther, B., Wolff, E.W., 2013. The Antarctic ice core chronology (AICC2012): an optimized multi-parameter and multi-site dating approach for the last 120 thousand years. Clim. Past 9, 1733–1748. http://dx.doi.org/10.5194/cp-9-1733-2013.
WAIS Divide Project Members, 2015. Precise interpolar phasing of abrupt climate change during the last ice age. Nature 520, 661–665. http://dx.doi.org/10.1038/nature14401.
Wolff, E.W., Chappellaz, J., Blunier, T., Rasmussen, S.O., Svensson, A., 2010. Millennial-scale variability during the last glacial: the ice core record. Quat. Sci. Rev. 29, 2828–2838. http://dx.doi.org/10.1016/j.quascirev.2009.10.013.
Wörner, G., 1999. Lithospheric dynamics and mantle sources of alkaline magmatism of the Cenozoic West Antarctic rift system. Glob. Planet. Change 23, 61–77.
Xiao, W., Frederichs, T., Gersonde, R., Kuhn, G., Esper, O., Zhang, X., 2016. Constraining the dating of late quaternary marine sediment records from the Scotia Sea (Southern ocean). Quat. Geochronol. 31, 97–118. http://dx.doi.org/10.1016/j.quageo.2015.11.003.